Technical Report
ALCEDO

Team 01 Technical Report to the 2024 EuRoC

Aerospace Team Graz (ASTG)
Graz University of Technology, Austria

Graz, September 15, 2024

Contact: m.ortner@astg.at

Abstract

The project ALCEDO is the second pressurized hybrid rocket built by ASTG, competing in the H9 (Student Researched and Developed (SRAD) hybrid 9 km) category at European Rocketry Challenge (EuRoC) 2024. Building on three successful years, ALCEDO aims to reach new heights and maintain our established professionalism. With improvements to the rocket and launch support equipment, we are eagerly anticipating this year's competition.

The launch vehicle closely resembles last year's HALCYON, with a 35 cm increase in length and an additional 10 kg in weight, resulting in a total length of 3.91 m and a launch weight of 41.5 kg. The payload consists of two CubeSats and the Demonstrator Attitude Determination System (DADS) payload. This payload is from Auroral Polarization EXplorer (APEX), demonstrating an attitude determination system for a future Rocket Experiment for University Students (REXUS) flight. The second CubeSat is provided by high school students, fostering the next generation of rocketeers. The third CubeSat from ASTG features a rotation-stabilized camera to capture parachute deployments.

The recovery section, below the nose cone, houses a dual recovery system with first- and second-stage deployment detection for in-flight feedback. The Avionics (AVI) stack, mounted similarly to previous years, includes the official tracking computer providing redundancy to our SRAD flight computer. The midsection contains the pressurizing tank, fluid assemblies, oxidizer tank, and various sensors. The servo-actuated main valve, burst disk, pressure and temperature sensors, and CANary are located below the oxidizer tank. ALCEDO also features an air brake with a compact design and the valvebay structure with an additional carbon thrust plate for transferring the thrust of the combustion chamber to the rest of the rocket. The ignitor was reiterated to achieve a more reliable ignition of the Hydroxyl Terminated Polybutadiene (HTPB) fuel grain. A flexible and replaceable 3D printed touchdown protection, protects the tailcone from damage on touchdown.

The launch support equipment has been upgraded to perform more robustly and reliably to keep up with the needs of ALCEDO. The flight computer Printed Circuit Board (PCB) offers enhanced data sampling, and the umbilical disconnection system has been reiterated for reliable detachment. Also part of our launch support equipment is our mission control, which features the overall control of the rocket and launch rail equipment, such as the Filling Station (FS). To ensure the performance needed, a dedicated server runs our mission control software.

Contents

1 Introduction

1.1 Team Introduction and Overview

The ASTG was founded in late 2019 at the Graz University of Technology (TU Graz) as a non-profit organization by a motivated group of students. Through the shared enthusiasm for the topics of rocketry and aerospace, the team quickly grew to over 85 members by 2024. During this time, multiple projects were carried out, and a lot of experience could be gained. One of the most rewarding moments in the team's history was the winning of the overall award for the HALCYON project at the 2023 EuRoC edition. In all of ASTG's participations in EuRoC, the launches and landings of our projects were characterized by obstacles. However, these experiences have awakened our ambition and boosted our drive to develop systems that perform flawlessly.

With very diverse fields of studies from all study levels, a good spectrum of different ages, and about one-fifth of the team consisting of women despite the challenges recruiting out of traditionally male-dominated fields of study, ASTG has the ability to take on even the most challenging projects and find new and innovative ways to solve problems. Figure 1.1 tries to highlight the diverse demographics of the team.

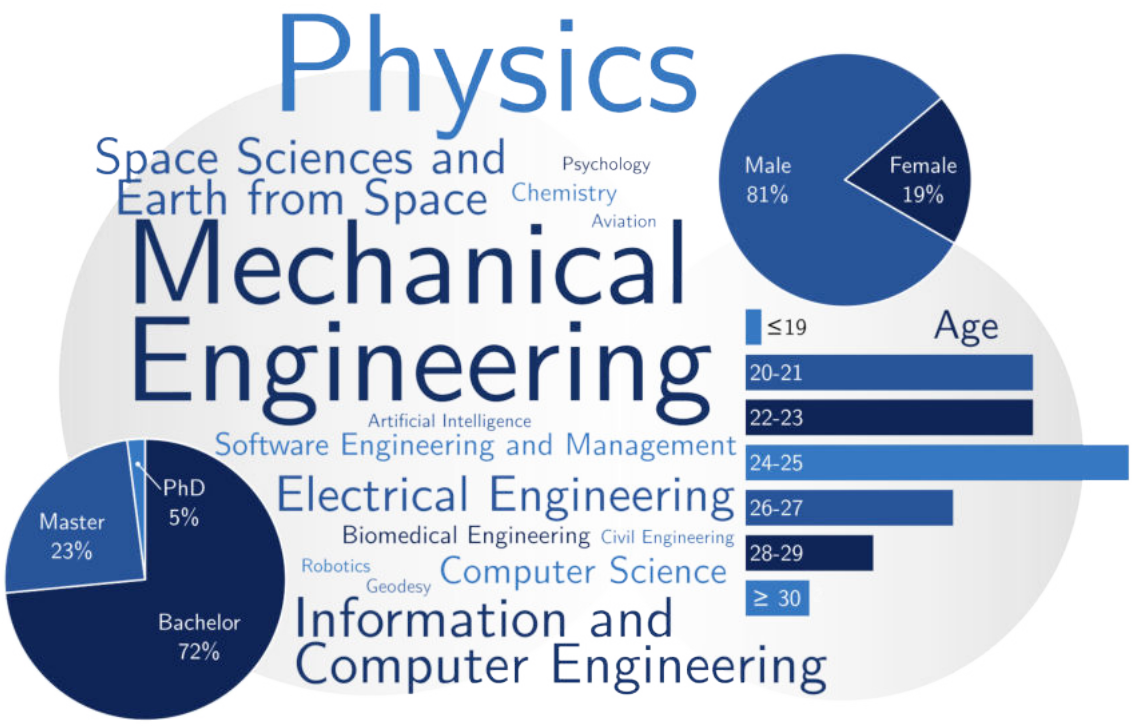

Figure 1.1: Overview of the team demographics showing study levels, gender distribution, the fields of studies, and age distribution.

1.2 Team Structure

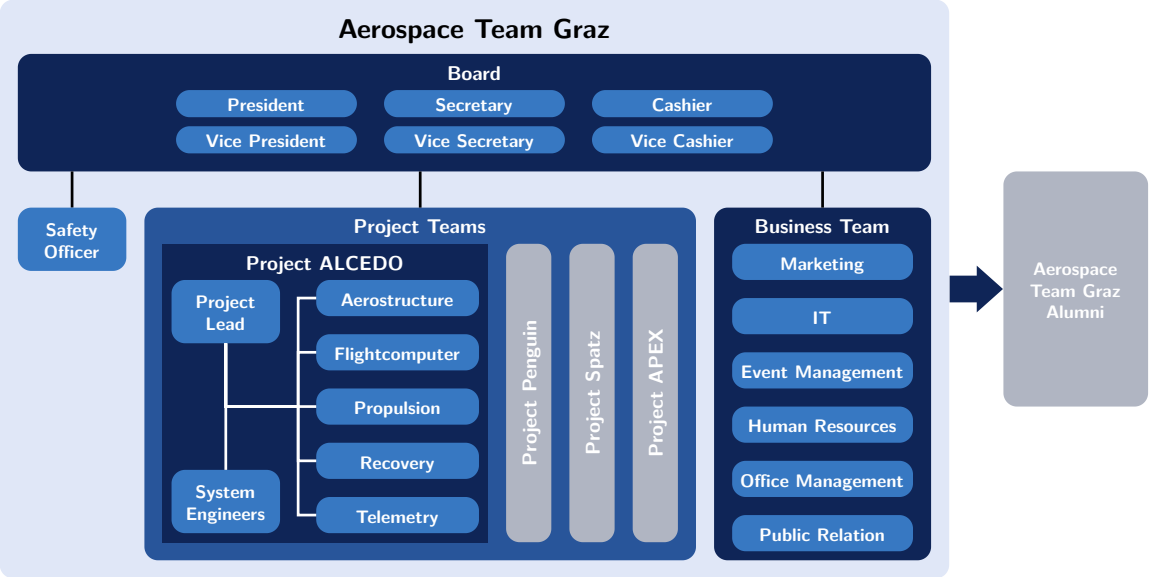

Figure 1.2: Organisational structure of the ASTG.

Figure 1.2 shows the organizational structure of the ASTG. Starting at the top, the Board is the elected leadership of the organization, deciding on the most critical matters and building and maintaining the necessary infrastructure and funds for the rest of the team. The Business Team works closely with the Board to manage administrative tasks, public relations, marketing, and human resources.

Continuing to the technical part of the organization: The team is split up into individual project teams. In the case of ALCEDO, the Project Lead, together with the Module Leaders and System Engineers, coordinates aspects such as time, resource, interface, risk management and project documentation.

As illustrated in Figure Figure 1.2, the project team is divided into five distinct modules, each responsible for their respective subsystems' design, engineering, and manufacturing. The Aerostructure Module (AST) focuses on the aerodynamics and structural components of the rocket, primarily working on the airframe, all connection points for the other systems, and the structural oxidizer tank. The Flight Computer Module (FLI) is tasked with enhancing the existing software and hardware for the SRAD flight computer. This includes gathering sensor data, actuating valves and other components within the rocket, and managing the Ground Support Equipment (GSE). To ensure reliable data transfer and actuation signals, the Telemetry Module (TEL) handles the necessary data links between the mission control, GSE, and the rocket, as well as position tracking via Global Navigation Satellite System (GNSS). The Propulsion Module (PRO) is responsible for the rocket's propulsion system, including all related components within the rocket and the GSE, particularly the FS and the horizontal test bed for Hot-Fire tests. Finally, the Recovery Module (REC) focuses on the dual deployment parachute system, including the development of testing facilities and custom-sewn parachutes.

1.3 Partners and Supporters

Despite the hard work and effort put in by all the motivated team members, realizing such a demanding project requires sponsorship and collaboration with numerous partners. The overall support is divided into contributions from educational institutions, public funds, and businesses in various forms, such as monetary donations, the supply of tools and materials, the provision of manufacturing capabilities, software licenses,

testing facilities, and the sharing of expertise and advice. Sponsors from this year include TU Graz, European Space Agency - Business Incubation Center (ESA-BIC), Federal Ministry for Climate Action, Environment, Energy, Mobility, Innovation and Technology (BMK), Institute of Production Engineering (IFT), Institute of Innovation and Industrial Management (IIM), Astotec Pyrotechnic Solutions, Peak Technology and over sixty more.

1.4 Project Goals

The goals for project ALCEDO were defined as:

- Create high-quality and comprehensive technical documentation as a foundation for future projects.
- Optimize and improve the design of our pressurized hybrid engine.
- Participate the first time in the history of ASTG in the 9 km flight category of EuRoC.
- Design and build a rocket capable of launching to either 3 km or 9 km, ensuring a successful campaign at EuRoC even if flight conditions prohibit a 9 km launch.
- Reach the top five at EuRoC'24.

1.5 Mission objectives

The mission objectives for ALCEDO were defined as:

- Carry the rocket's payload with a total mass of 2.5 kg to the desired altitude. The payload consists of two 1U (high-school) student build CubeSats and an additional payload containing an altitude determination system demonstrator for glsapex, a glsrexusbexus project to the desired altitude.
- Complete a nominal flight from a successful launch to a safe recovery of ALCEDO.
- Reach an apogee of 9 km as exactly as possible by deploying the air brake as needed.

2 Launch Vehicle System Architecture

2.1 Overview

The subsystems of the launch vehicle are distributed across five modules, with the integrated systems depicted in Figure 2.1. Not every component is detailed due to the tight integration necessary for the vehicle's compact design.
Starting from the top, the nose cone contains the payload consisting of two 1U CubeSats and the DADS. The nose cone is mounted via the coupling tube and secured with shear pins. During the first stage of the dual deployment REC, the nose cone is separated from the rocket. The REC system consists of two individual parachutes, the drogue parachute and main parachute, both are sewn in-house. The deployment systems are updated versions from previous projects and adapted to the needs of ALCEDO. Additionally, two cameras are installed in this section to capture both deployment events.
Below that, the AVI section with the SRAD flight computer and TEL antenna system forms the upper part of the midsection. The flight computer controls actuators, reads out sensors, and monitors the battery inside of the launch vehicle. In the midsection, three splitters for the three distinct patch antenna rings are mounted, enabling the wireless data transfer link and the GNSS positioning. The midsection includes two radial cameras to capture the flight. Right below the AVI mount, the propulsion system with the nitrogen pressurizing tank, pressure regulator, vent valve, and a dip tube for the 9 km fill level of the oxidizer, the nitrogen fill port and the control and sensor PCB are located, summarized under upper fluid assembly in Figure 2.1. Right below that, the structural oxidizer tank with the lower fluid assembly, including a servo-actuated main valve, burst disk, multipoint thermocouple, pressure sensor, manual relief valve, vent valve for the 3 km fill level, and the nitrous oxide fill port are located. This part is connected via the valve bay structure to the air brake. The feedpipe extends from the lower fluid assembly through the air brake into the combustion chamber, which is mounted via the valve bay structure, made of aluminum and carbon fiber tubes, to the air brake, which transfers the thrust to the rest of the launch vehicle. The combustion chamber consists of a swirl injector, pressure sensor, ignitor, HTPB fuel grain, and a mixing device to further enhance the combustion and the nozzle at the end. All that is enclosed by the tail cone, which features a touchdown protection made of Thermoplastic polyurethane (TPU) and a downwards-facing camera.

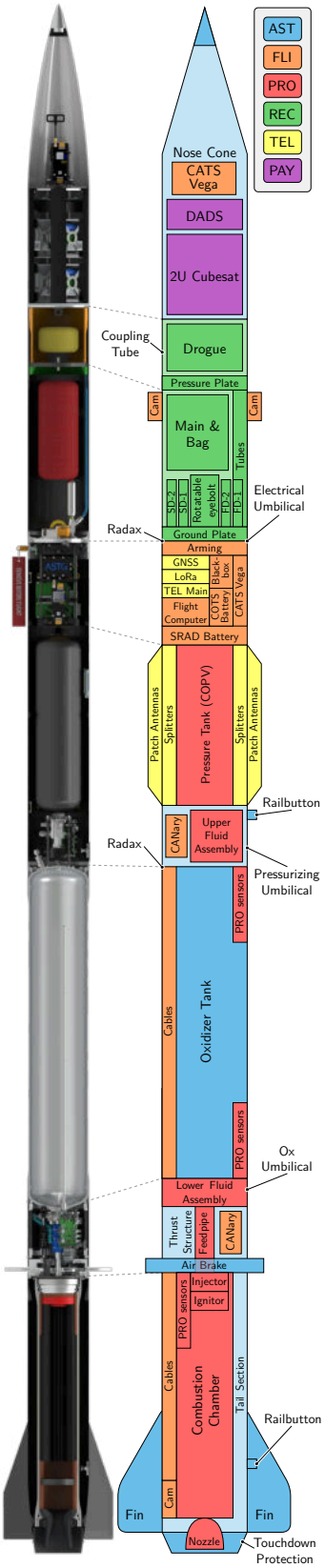

Figure 2.1: Overview of the launch vehicle and partitioning of major subsystems.

2.2 Propulsion Subsystem

The primary objective at the beginning of ALCEDO's engine development was to enhance the previous year's pressurized hybrid system by increasing integration and reliability, with the goal of achieving a 9 km apogee. The rocket utilizes nitrous oxide (N_2O) as the oxidizer and HTPB as the fuel, with nitrogen (N_2) used as the pressurizing gas. The propulsion stack, as depicted in Figure 2.2, is divided into two primary assemblies: the oxidizer tank assembly and the combustion chamber. The oxidizer tank assembly is further subdivided into the pressurant tank, the upper fluid system, the oxidizer tank, and the valve bay. The air brake is situated between these two major assemblies. Further details on the combustion chamber are provided in Section 2.2.2.
Nitrous oxide (N_2O) is selected as the oxidizer over liquid oxygen (O_2) for several reasons. Firstly, the aim is to maintain consistency with last year's engine design. Secondly, the logistics of managing liquid oxygen without appropriate gas storage infrastructure present significant challenges. While efforts are underway to establish proper gas storage for future projects, it was not feasible for this year's project.
The fuel options considered were paraffin, as used last year, and a HTPB-based mixture. Early in the development process, two Hot-Fire tests with paraffin and three with HTPB were conducted. The HTPB tests demonstrated improved stability, leading to its selection as the fuel. To address the lower regression rate of HTPB, a finocyl grain geometry is chosen, achieving an oxidizer-to-fuel ratio between 7 and 8 This ratio aligns with the theoretical maximum efficiency, calculated using National Aeronautics and Space Administration (NASA)'s Chemical Equilibrium with Applications (CEA) tool [**Gordon1976ComputerDetonations**].

Table 2.1: Engine characteristics.

Characteristic	Value
Length	2.20 m
Pressurant Tank Pressure	300 bar
Oxidizer Tank Pressure	55 bar
Combustion Pressure	25 bar
Total Impulse	24 250 Ns
Burn Time	8 s
Oxidizer Mass	11 200 g
Fuel Mass	1650 g
Empty Mass	12 430 g

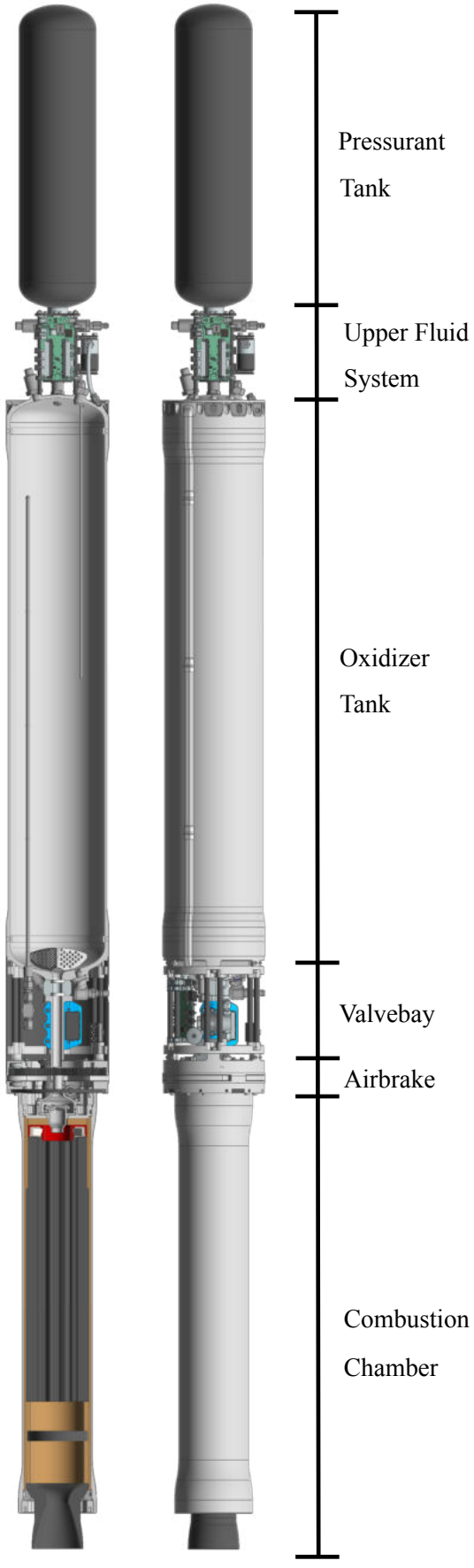

Figure 2.2: Sections of the Propulsion Stack.

2.2.1 Fluid System

The fluid system is centered around the structural oxidizer tank. The upper fluid system is positioned above the oxidizer tank, which supplies the pressurant gas to the oxidizer tank during the burn. This configuration enables faster launch readiness compared to a self-pressurizing system, as it eliminates the need to wait for the oxidizer to reach the required pressure. Additionally, the system ensures a more stable thrust curve throughout the burn by maintaining constant pressure in both the oxidizer tank and the combustion chamber. The pressurant tank is connected to the oxidizer tank via a pressure regulator, which is set to a static pressure of approximately 55 bar.

An additional advantage of pressurization is the ability to operate at lower temperatures. By achieving temperatures of −20 °C, a higher density is reached, minimizing the needed tank volume, therefore saving space and reducing weight. The low temperatures are achieved through a new tanking procedure in which the oxidizer is expanded at the fill valve, reducing the pressure to 18 bar which equals a temperature of −20 °C.

The system has the ability to switch between an 9 km and an 3 km apogee if the weather makes it necessary. This is accomplished using two vent valves, one located at the top and one at the bottom of the tank. To achieve precise tanking for either option the two vent valves have dip tubes attached which differ in length to manage the two required oxidizer levels. The bottom vent valve also serves to speed up the tanking procedure and gets closed as soon as liquid venting is visible. Two Quick Disconnect (QD) arms, which can be disconnected independently via the mission control, are utilized for tanking and pressurizing the rocket.

To enhance the safety of the system, a range of options for depressurization are available. The primary option is to open both vent valves via the mission control. In the event that the mission control retains control of the rocket but is unable to access the vent valves, the next option is to open the main valve and dump the oxidizer through the combustion chamber. In the event of a loss of control by the mission control, launch site personnel can electrically override the lower vent valve. An additional key switch at the ignition box, located 15 m from the rocket, actuates the lower vent valve, provided that the electrical umbilical is still connected and the filling station has power. The next option would be to open the manual bleed valve, although this would only be a viable option if the pressure is below a certain threshold where it is safe to approach the rocket. As a final measure, if no other options are feasible, the system will rely on the pressure increasing until the burst disc opens.

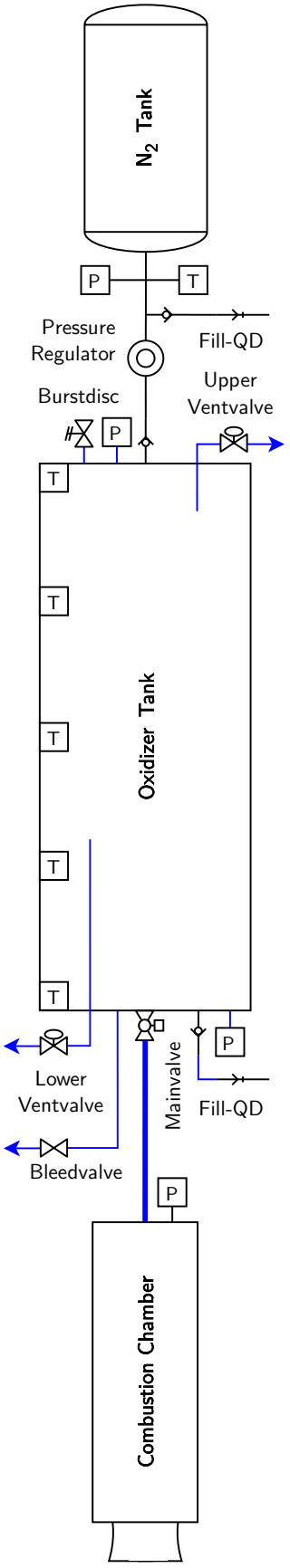

Figure 2.3: Fluid system of the rocket.

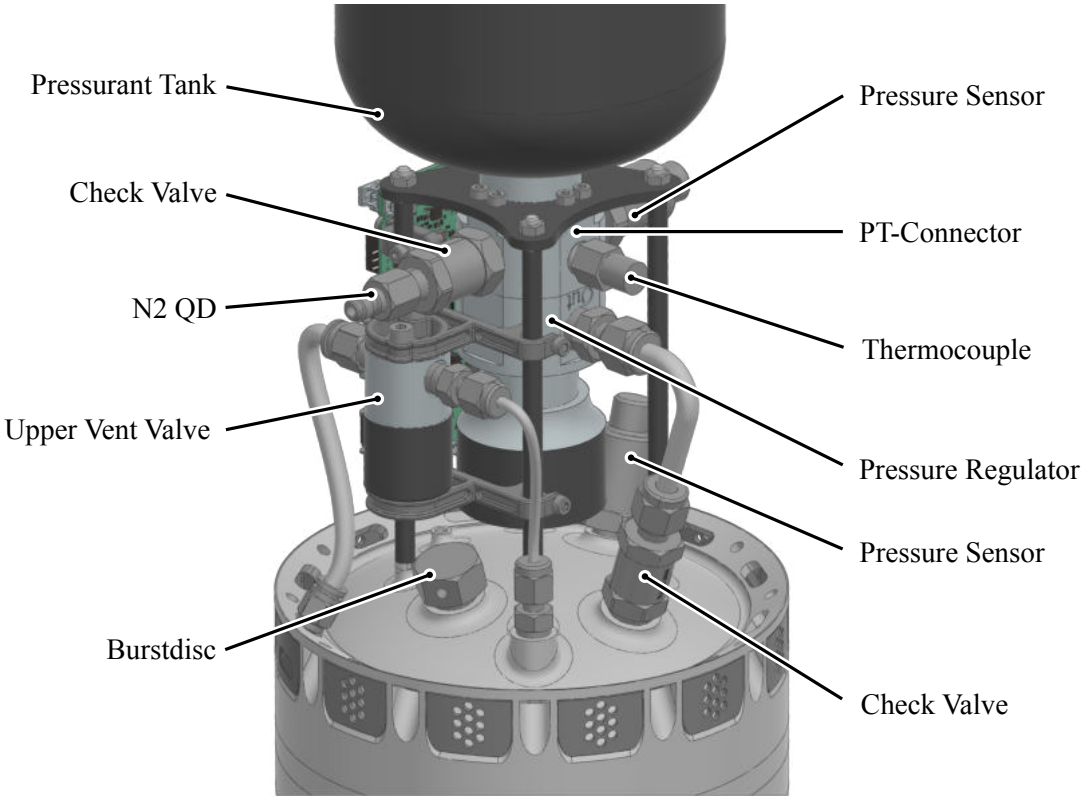

Figure 2.4: Shown is the upper bulkhead together with the upper fluid system.

Upper Fluid System

The pressurant tank connector (PT-connector) forms the core of the upper fluid system, linking the pressurant tank, a pressure sensor, a thermocouple, a check valve with the QD, and the pressure regulator. It is mounted beneath a carbon plate, which is attached to the oxidizer tank using carbon tubes and thread inserts. A critical component of this system is the connection between the PT-connector and the pressure regulator. The bottom of the pressure regulator features a drilled hole that interfaces with the PT-connector, sealed with an O-ring. This allows to reduce weight and save space by eliminating the need for additional piping and connectors. The connection to the oxidizer tank is achieved via a check valve, which is directly screwed into the bulkhead of the oxidizer tank, ensuring that no oxidizer can enter the high-pressure system.

Oxidizer Tank

The oxidizer tank has an internal volume of 12.79 L, with a nominal ullage in flight configuration of 1.5 L. The design pressure of the tank is 120 bar, with a nominal operating pressure of 60 bar with a resulting dry weight of 4.57 kg. The tank is constructed from two end caps and a cylindrical section made of AL 6082 T6. The individual parts are joined by two TIG U-Welds using ER5356 filler material. The cylindrical section has a thickness of 3.4 mm with an increased thickness at the welds of 6.2 mm. Each weld is centered by a backing ring, ensuring concentricity between the components and allowing for complete penetration of the weld. After the welding process, the tank was then turned to the final diameter. The bulkheads have a torispherical profile, which, in contrast to the previously used ellipsoidal shape, shows a more favorable stress distribution in the area of the ports and the welds, permitting a reduced wall thickness. The profile is also shallower, increasing the available internal space.

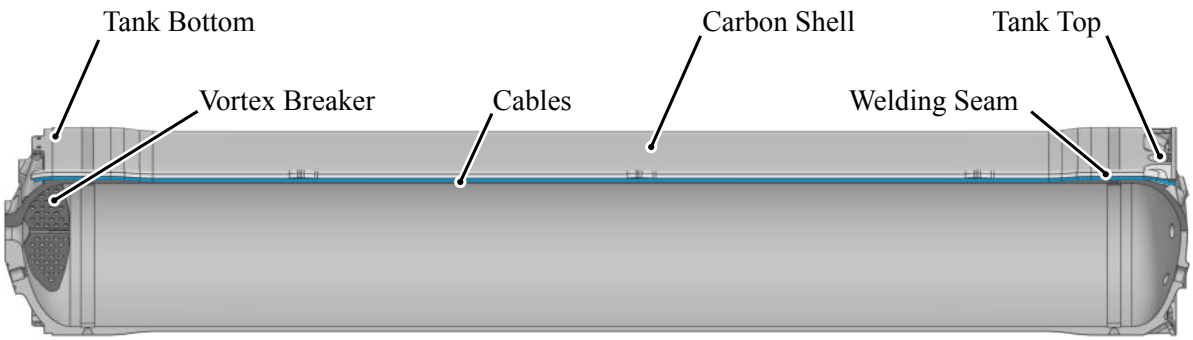

Figure 2.5: A cutaway view of the oxidizer tank.

The general design philosophy was carried over from previous flight tanks and consists of two main aspects: Firstly, make the tank a structural component of the rocket. Secondly, keep the fluid system plumbing at a minimum through a fully integrated construction.

The first aspect is achieved by making the tank the same diameter as the rocket and integrating structural mounting points into the tank itself. On the upper bulkhead, a Radax joint is directly integrated into the bulkhead and connects to the midsection shell. Similarly, the pressurizing system also mounts directly to the upper bulkhead. The lower structural connection consists of a bolted flange for the valve bay structure. The second aspect was realized by mounting all components of the fluid system directly to the tank. Each sensor, valve, and other component has a dedicated port in the bulkhead.

As seen in Figure 2.4 and Figure 2.6, the upper bulkhead features ports for the upper pressure sensor, the pressurizing check valve, the upper vent valve, and the burst disc. The lower bulkhead has an interface for directly mounting the body of the main valve, the lower pressure sensor, the lower vent valve with dip tube, the manual relieve valve, and the multipoint thermocouple. The N_2O QD is also mounted directly to the bulkhead, with a threaded check valve integrated into the tank.

The first Hot-Fires with a test tank of similar volume showed disturbances consistent with the formation of a vortex and intermittent ingestion of gaseous oxidizer. In order to suppress the formation of a propellant vortex, two perforated plates were welded to the lower bulkhead at the bottom of the tank. Subsequent Hot-Fire tests with the vortex breakers installed did not show any further anomalies.

While the integrated construction increases the geometric complexity of the bulkheads, it allows for a reduction the required piping for both upper and lower fluid assemblies to a minimum, saving weight and internal space. On a system level, self-conducted concept studies have concluded that for the current tank volume, a composite tank would not yield significant weight savings because even though the tank itself is substantially lighter, it requires additional plumbing, mounting hardware, and structural interfaces, which diminish the possible weight reduction. Due to all fluid system components being mounted directly to the tank, the whole fluid system is self-supported and self-contained. This reduces the complexity of integrating the propulsion system with the rest of the rocket.

Main valve

The main valve consists of a 3-piece 3/4” Commercial-off-the-shelf (COTS) ball valve. The COTS flanges of the valve are fully integrated into the system, which significantly reduces the system weight and required space. The top flange is integrated into the aluminum bulkhead of the oxidizer tank. The lower flange is integrated into the feed pipe, which connects the valve to the combustion chamber. When compared to a standard solution with fittings and piping, this design saves over 50 % weight. The valve is actuated by a servo using a four-bar linkage. This four-bar linkage provides a variable transmission with the highest

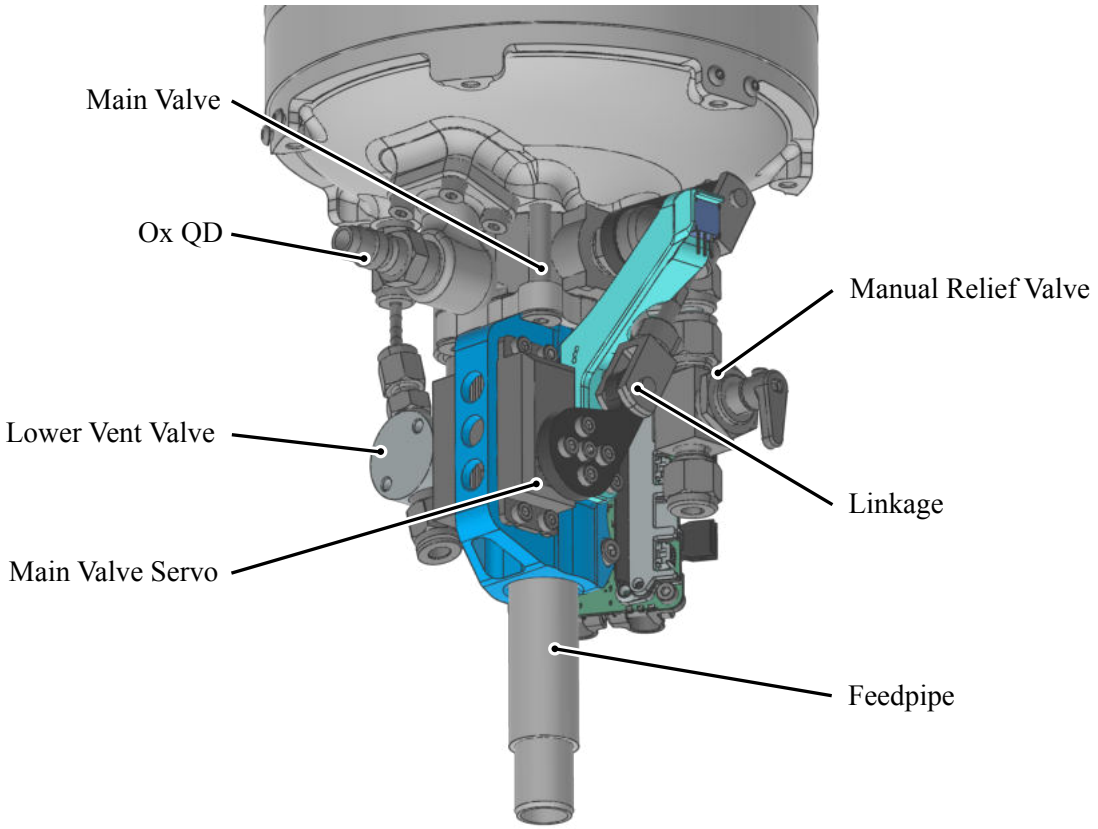

Figure 2.6: The lower bulkhead and the lower fluid assembly with the main valve and the feed pipe.

ratio at the end positions, which helps to overcome the breakaway torque. The valve position is monitored by a potentiometer directly connected to the shaft of the ball valve.

2.2.2 Combustion Chamber

Structure

The outermost layer of the combustion chamber is a cylindrical aluminum EN AW 6082-T6 casing, the material was chosen for its high strength so the weight can be minimized. The tube is anodized to increase its surface hardness, thereby improving its durability against wear and scratches. Both ends are threaded to facilitate assembly and feature a smooth cylindrical face further inwards for sealing the combustion chamber with an O-ring.

The combustion chamber is closed off at the top by the bulkhead, an aluminum disc which acts as a durable interface between the combustion chamber and the injector as well as the injector cover. Additionally, a pressure needle allows a pressure sensor to be connected to the combustion chamber, enabling engine performance monitoring and simplifying troubleshooting in case of a malfunction.

A recess on the bulkhead's outside allows for the fuel grain to be constrained by the bulkhead both radially and axially. The injector outlet sits in a tight fit with the central bulkhead hole which includes an O-ring notch for sealing. On the top of the bulkhead are six screw holes for mounting the injector cover.

The injector cover features an O-ring groove on the outside to seal the interface with the bulkhead and two more on the top where the feedpipe is inserted. It features a conical transition to the larger injector diameter. When the injector cover is screwed to the bulkhead, a small gap remains between them. This way, the injector cover presses tightly against the injector and holds it in place axially.

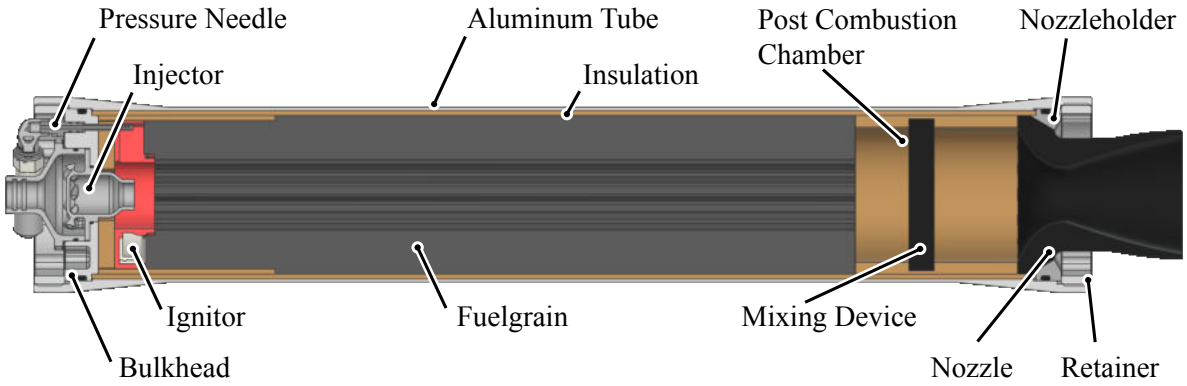

Figure 2.7: Depicted is the combustion chamber with its components. Starting from the left with the injector cover and the injector in the bulkhead held in place by a retainer. Then the ignitor on top of the fuel grain. After the fuel grain the post combustion chamber with the mixing device and at the end the nozzle with the nozzle holder and a retainer.

At the other end, the combustion chamber is enclosed by the graphite nozzle, a Laval nozzle with a converging and a diverging section. The nozzle is secured by the fuel grain insulation and a nozzle holder, which is held in place against the combustion chamber pressure by a threaded retainer ring. The conical interface between the nozzle and the nozzle holder in combination with graphite paste seals the combustion chamber at the lower end. Additionally an O-ring seals the interface between the nozzle holder and tube.

The inside of the casing is lined with the fuel grain insulation, which is tightly fit into the casing and firmly kept in place by screwing on the retainers onto both ends. The retainer also features eight screw holes to connect the combustion chamber to the air brake structure via a carbon thrust plate, which is further detailed in Section 2.3.1.

Injector

The injection system of ALCEDO consists of a single element swirl injector and is responsible for injecting the oxidizer into the combustion chamber. It also limits the flow of oxidizer to achieve the correct ratio of fuel to oxidizer and ensures good atomization of the oxidizer, leading to a more efficient combustion. In swirl injectors, the oxidizer enters the body of the element through tangential ports leading into a swirl chamber. The tangential velocity imparts a rotational motion onto the oxidizer and forms a swirl. The oxidizer spirals down the length of the swirl chamber, where the nozzle further contracts the flow, leading to higher tangential velocities and the formation of a thin sheet of oxidizer. Upon exiting the nozzle into the combustion chamber, the liquid sheet breaks up and forms a conical spray, which impacts the fuel grain. Swirl injectors generally have favorable atomization properties, leading to a reduction of combustion instabilities, and have been shown to increase regression rate in hybrid rocket engines [**Heydari2017ExperimentalMotor**].

Current modeling for swirl injection lacks general applicability, especially for high vapor pressure propellants such as nitrous oxide, and therefore, it was decided to pursue a more empirical approach. Different injectors with varying geometry were coldflowed with a mass flow sensor and a coldflow chamber, simulating the combustion pressure. CO_2 was used as a substitute for N_2O as it shows similar properties with reduced environmental impact [**WaxmanMassRockets**]. The most promising candidate was then scaled to fit the engine and further refined during the Hot-Fire campaign.

The flight injector features six inlet ports with a diameter of 3.58 mm, a swirl chamber diameter of 20.57 mm and a nozzle diameter of 12.52 mm. The measured discharge coefficient of this injector in the horizontal Hot-Fires was (0.20 ± 0.01)

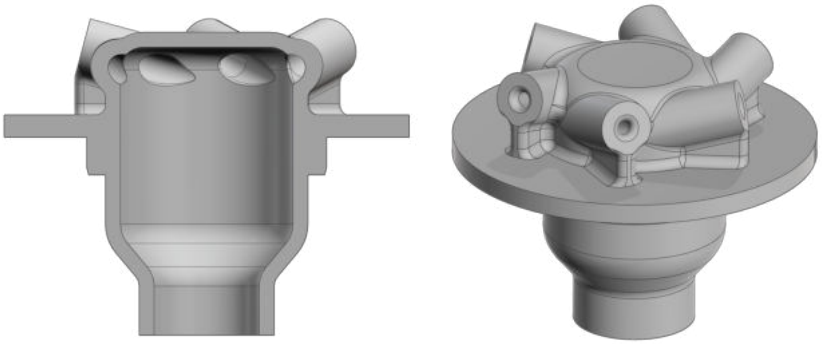

Figure 2.8: The left image shows a cutaway of the swirl injector, the right one an isometric view.

The Hot-Fire tests in flight configuration initially showed severe, low-frequency instabilities at 50 to 59 Hz and amplitudes of 12 bar. The cause of the instabilities was determined to be the significantly shorter feed system in flight configuration with reduced hydraulic losses and therefore less inherent damping compared to the horizontal test setup. The frequency and occurrence of the instabilities were consistent with feed system coupled ”chugging” instabilities. The solution was to improve the decoupling of the feed system and combustion chamber by increasing the pressure drop across the injector from the initial 7 bar to 11 bar. Further Hot-Fires showed that this measure effectively reduced those instabilities.

Fuelgrain

The hybrid engine was initially designed to operate on various fuels. In the early stages of development, initial tests using paraffin wax and HTPB were conducted. The test saw five Hot-Fire tests successfully conducted, with the same combustion chamber layout and fluid setup. Both tests with paraffin showed major instabilities in thrust and combustion chamber pressure, whereby all three tests with HTPB showed very consistent and efficient combustion.

To ensure the new fuel meets the necessary performance criteria numerous tests were conducted using different formulas. The final fuel composition is based on HTPB and includes the following components:

- 90 % HTPB: The primary fuel and binder.
- 9 % Isophorone diisocyanate (IPDI): The curing agent.
- 1 % Coal powder: Added to improve thermal radiation absorption, ensuring uniform combustion across the fuel grain’s surface and minimizing thermal stress on the combustion chamber.
- 0.015 % $Fe(AcAc)_3$: A catalyst that reduces the curing time.

The liquid fuel mixture is gravity-cast directly into the phenolic resin cotton insulation and cured at 65 °C in an oven. After removing the core, the resulting fuel grain has a finocyl geometry as shown in Figure 2.9. This shape was chosen over a hollow cylinder design to increase the burning surface area and is necessary to compensate for the fuel mixture’s low regression rate, ensuring the combustion meets the required oxidizer-to-fuel (O/F) ratio. Further efforts were made to enhance the performance, including experiments with other additives like copper powder, lecithin, expandable graphite or silicon oil. However, the improvements were minimal, leading to the decision to abandon these approaches.

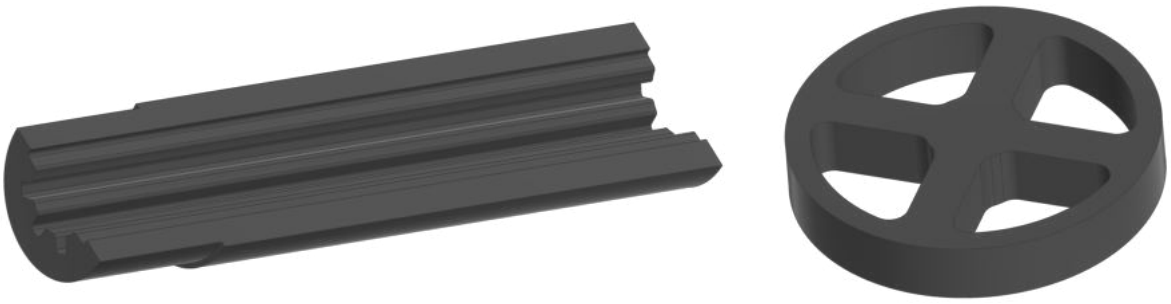

Figure 2.9: Cross section of the Fuel Grain and the mixing device which are used in the combustion chamber. The mixing device is made out of carbonized carbon, the fuelgrain a HTPB mixture.

Mixing Device

The purpose of the mixing device is to create turbulence in the combustion gases, thereby enhancing the mixing of N_2O and fuel. This improved mixing directly contributes to increased combustion efficiency, as documented by [**Hill2022EvaluationDevice**] and confirmed by the test campaign results. To endure the high temperatures and abrasion present during operation, the mixing device is constructed from carbonized carbon plates. The device consists of an outer ring and an inner plate, connected by four radial struts as depicted in Figure 2.9. The holes in the device are designed to be slightly larger than the initial port area of the fuel grain, minimizing any significant pressure drop. The mixing device is positioned one-quarter of the way down the post-combustion chamber from the fuel grain.

Ignitor

The ignitor of the combustion chamber sits on top of the fuel grain, around the injector. It has a toroidal shape with a flame guide aimed along the port of the fuel grain, to preheat and vaporize parts of the fuel evenly along the whole port length and circumference. The ignitor consists of three 3D printed parts, as can be seen in Figure 2.10. The inner two form a C-shaped chamber with a port toward the inside. The chamber is filled with about 30 g of a pyrotechnic mixture consisting of 60 % rocket candy (65 % potassium nitrate and 35 % sorbitol), 25 % CaSi powder and 15 % magnesium powder. The metal powders produce hot sparks, while the rocket candy acts as a binder and expulsion charge. The last 3D-printed part acts as a flame guide, diverting the sparks along the fuel port. The pyrotechnic mass is ignited with four e-matches for redundancy.

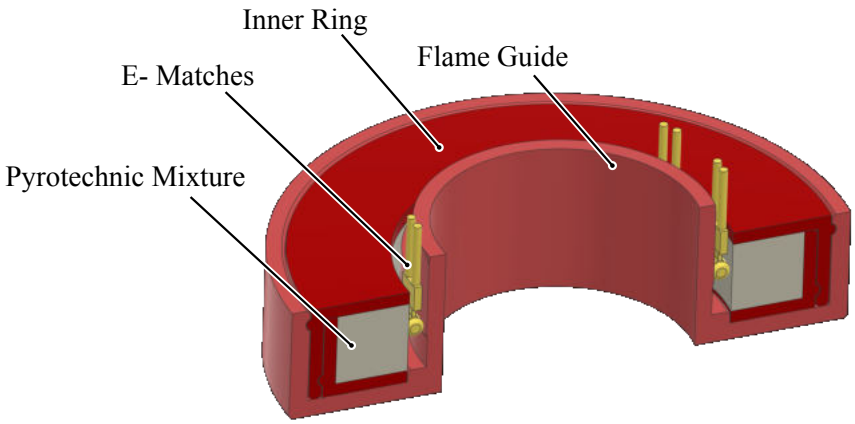

Figure 2.10: Depicted is the ignitor in a cutaway section. The inner ring houses the pyrotechnic mixture, the base allows for four e-matches to be placed and provides the flame guide.

2.2.3 Testing

To achieve a reliable propulsion system, an extensive testing campaign was conducted. Commencing with the hardware of last year's rocket HALCYON, a new tanking scheme was explored in a Cold-Flow. For this, the filling station was adapted to fit the newly developed procedure. With the concept proven, the first Hot-Fires were conducted successfully using old hardware. To gain additional information, a flow measurement was implemented in subsequent tests, thereby allowing a more detailed examination of injector characteristics. At this point, a decision was made to move to HTPB instead of paraffin as fuel, due to a more stable burn as seen in various Hot-Fires.

At the fourth Hot-Fire difficulties were encountered at ignition, which was attributed to incorrect storage of the ignitor. In the same test, three nozzles broke while firing, which can be most likely attributed to a combination of faulty manufacturing and an overly optimistic nozzle design. As a result, the nozzles were reiterated to include a higher safety margin. The next tests showed the improved nozzles survived even strong instabilities. Furthermore, some vertical tests failed because of a wrong linkage used for the connection between the main valve and its servo motor. This failure only was present for one of two flight configuration propulsion stacks, the other stack operated normally but was not used for this test to prove both stacks were ready for flight.

In total, eleven horizontal and three vertical Hot-Fires were sucessfully conducted. The relevant successful paraffin and HTPB Hot-Fires are listed in Table 2.2. Tests 1.3, 4.1, and 4.2 with failed ignitions are not listed. As are the Hot-Fires 6.2 and 7.1 in which the main valve failure occurred and no nominal thrust could be achieved.

Table 2.2: Summary of the ALCEDO Hot-Fire campaign. F_{max} signifies the peak thrust, I_{tot} the total impulse, m_{ox} the oxidizer mass and t the burn time.

Hot-Fire	F_{max} [kN]	I_{tot} [kN · s]	m_{ox} [kg]	t_{burn} [s]	Notes
HF 1.1	3.8	9.4	4.8	3.2	Paraffin
HF 1.2	4.1	13.1	6.3	3.9	Paraffin
HF 2.1	4.2	17.6	7.1	4.8	HTPB
HF 2.2	4.3	16.4	7.3	4.5	Paraffin
HF 2.3	4.3	17.8	7.3	4.9	HTPB
HF 2.4	4.3	16.8	6.9	4.7	HTPB
HF 2.5	4.2	17.0	7.2	4.8	Paraffin
HF 3.1	4.3	18.6	8.2	6.0	HTPB
HF 3.2	4.2	19.7	8.1	6.5	HTPB
HF 3.3	4.2	21.3	9.7	7.1	HTPB
HF 4.3	4.0	22.7	10.3	8.5	HTPB
HF 5.1	3.8	18.6	10.7	6.8	HTPB, vertical
HF 5.2	4.5	7.1	3.6	1.9	3 km HTPB, vertical
HF 6.1	4.0	23.1	10.7	7.3	HTPB, vertical

2.3 Aerostructure Subsystem

The airframe of the rocket is made out of the following airframe sections.

- **Nose cone shell:** Houses the payload.
- **Recovery shell:** Houses the parachute and its systems.
- **AVI shell:** Houses the flight computer, upper fluid assembly, and the pressurant tank.
- **Valvebay structure:** Houses the lower fluid assembly.
- **Tail cone shell:** Houses the booster, and connects to the fins.

Stability is provided by four carbon fins and an air brake can actively control the apogee of the rocket. After structural integrity, which is confirmed either via analytical calculations, Finite Element Analysis (FEA) or testing. The main design considerations aim to minimize weight and drag, improve integration time, and make the production more cost- and work-efficient. Furthermore, a good characterization of the rocket's drag properties through Computational Fluid Dynamics (CFD) allows for accurate flight simulations.

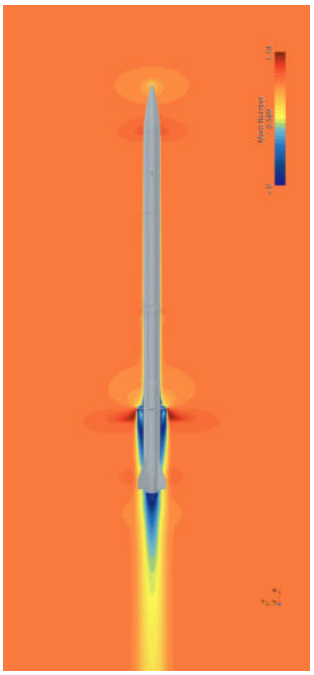

Figure 2.11: Air flow field image around ALCEDO

2.3.1 Structure

Shell

The shell is wound with Carbon-fiber Reinforced Polymer (CFRP), and the lay-up of the AVI shell is listed in Table 2.3. Depending on the payload need regarding Radio Frequency (RF) transparency the lighter CFRP nose cone can be replaced by a Glass-fiber Reinforced Polymer (GFRP) nose cone.
To prove that the structural integrity under the expected loads is given, the classical laminate theory was used with AltairESAComp™. To confirm the results a FEA as well as a bending test were performed. In Table 2.3 the lay-up for the AVI shell is given. Theoretically, the lay-up has a final thickness of 1.15 mm with a total of eight layers. After curing, the wall thickness of the tube was measured to be slightly above 1.2 mm, therefore it was sanded down to 1.2 mm in order to gain a smooth surface.

Table 2.3: Properties of the wound AVI shell.

CFRP	Lay-up [°]	Layer Thickness
T800	+/-89	0.26 mm
T800	0	0.125 mm
CC75	45	0.085 mm
T800	0	0.125 mm
CC75	45	0.085 mm
T800	+89	0.26 mm
T800	0	0.125 mm
CC75	45	0.085 mm
T800	+89	0.26 mm

Strain Gauge

The forces acting on the rocket's shell can only be estimated before a flight. In order to optimize the weight of the shell for future projects, the deformation of the rocket's shell due to bending around the two short axes of the rocket is measured. Therefore eight strain gauges in two 90° rotated Wheatstone bridges are installed on the inside of the AVI shell.

By measuring the changes in resistance of a conductive material inside of the strain gauge, a voltage difference is measured when the tube is bent. The configuration of the bridge is given in Figure 2.12. This configuration cancels out the deformation of the shell caused by a normal force. A setup to measure the normal strain on the rocket's shell was experimented with but did not deliver promising results.

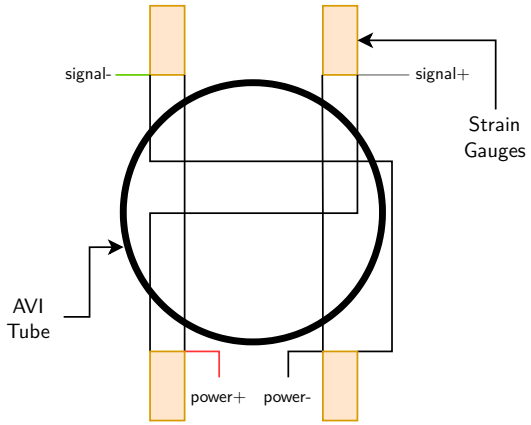

Figure 2.12: Diagram of one Wheatstone bridge with four strain gauges.

Payload Structure

The nose cone shell functions as the enclosure for the CubeSat payload and the option of mounting the Control and Telemetry Systems (CATS). The payload and flight computer are mounted on four rails, which are made from 3D-printed Polyactic acid (PLA) material. This setup allows for easy integration of these subsystems by sliding them into the nose cone shell. In the axial direction, the payload is constrained via a CFRP ring located at the front of the payload stack, which is attached to the shell with epoxy adhesive.

At the rear, the payload stack is supported by the payload retainer, which features an isogrid structure on its surface and is fastened to the lower CFRP ring with eight screws. This retainer not only supports the payload but also forms a seal between the first deployment pressure chamber and the nose cone. Additionally, it includes a stainless steel swivel for connecting the nose cone to the drogue parachute and an acrylic glass window to provide the lower of the two CubeSats with an unobstructed view of deployment events.

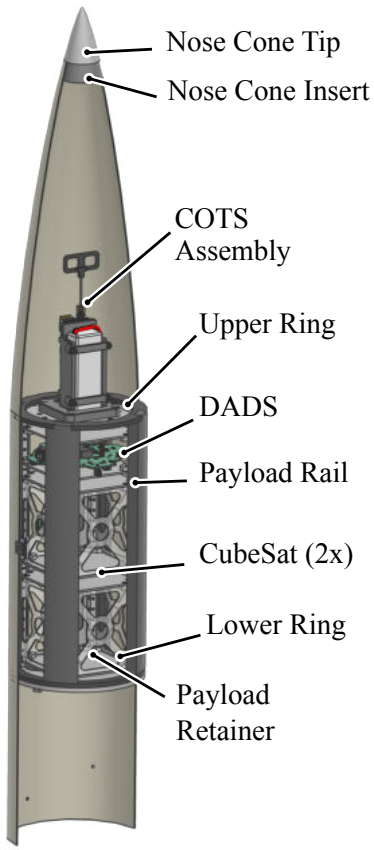

Figure 2.13: Section view of nose cone section with the payload section

Coupling Tube and Pressure Chamber

The connection of the nose cone and recovery section is separated at apogee to allow for the parachute deployment. The connection is realized with a coupling tube wound out of CFRP, which has a wall thickness of 1.5 mm. The coupling tube's outer surface forms a tight fit with the inner surface of the nose cone shell, and on the opposite side, is adhered to the inner surface of the REC shell. To secure the nose cone to the rocket body, three M2.5 nylon shear bolts are screwed in radially through the nose cone shell and the coupling tube. The payload retainer from Section 2.3.1 seals the top of the pressure chamber. A CFRP plate forms the bottom end of the chamber, sitting on top of a CFRP and Acrylonitrile Styrene Acrylate (ASA) ring. In Figure 2.22 the pressure chamber is rendered.

Radax

Two major connection points in the rocket are realized through Radax joints. Both Radax joints provide attachments to the avionics section, connecting it with the recovery section at the top and the oxidizer tank at the bottom. Apart from the tank, each Radax joint is bonded to its respective shell with epoxy adhesive. Twelve M4 screws secure the joint, which features a conical interface between the halves for self-centering and alignment during screw tightening.

What makes the Radax joint stand out from other alternatives is that it occupies minimal internal space, allowing for large interior assemblies while maintaining high joint stiffness and low weight.

Furthermore, the joints provide mounting points, such as for the recovery ground plate through an inner flange with screws. To provide the avionics section with access to correct pressure data, each female part of the joint has an arrangement of small holes between each screw. The holes also allow the flight computer's fan to provide adequate cooling.

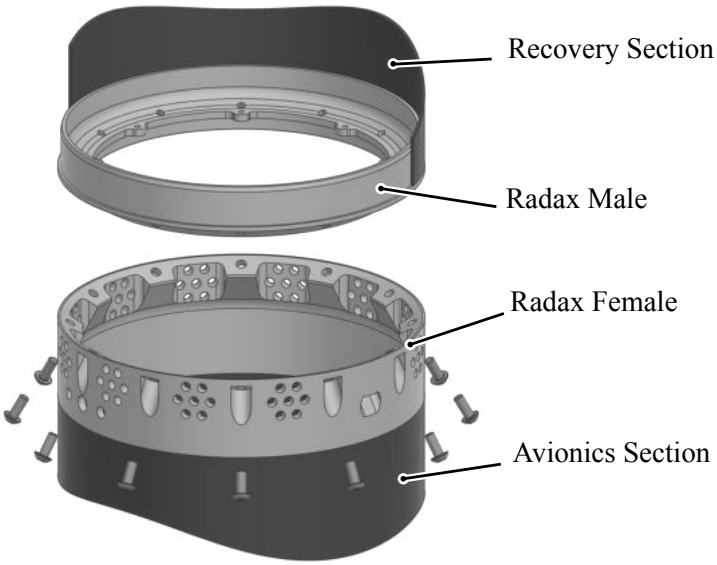

Figure 2.14: Upper Radax joint.

Valve Bay Structure

To allow easy access to the main valve of the fluid system and its surrounding components, the area between the air brake and the oxidizer tank is not covered by a continuous tube like the rest of the body, but rather by three individually removable carbon panels. Instead of the outer shell, the transfer of force and structural integrity is maintained by the valve bay structure, which consists of two circular aluminum frames connected by carbon rods. It connects to the air brake on one end and to the oxidizer tank on the other, providing a secure connection and ensuring that no force is transmitted onto the fluid system's valve.

The carbon rods are capable of withstanding the forces generated by the propulsion system while minimizing weight and also keeping a small footprint so they do not obstruct the path to the fluid system components when access is needed. They also act as a mounting rack for the fluid system's CANary, whose connectors can also be easily reached when the corresponding outer panel is removed.

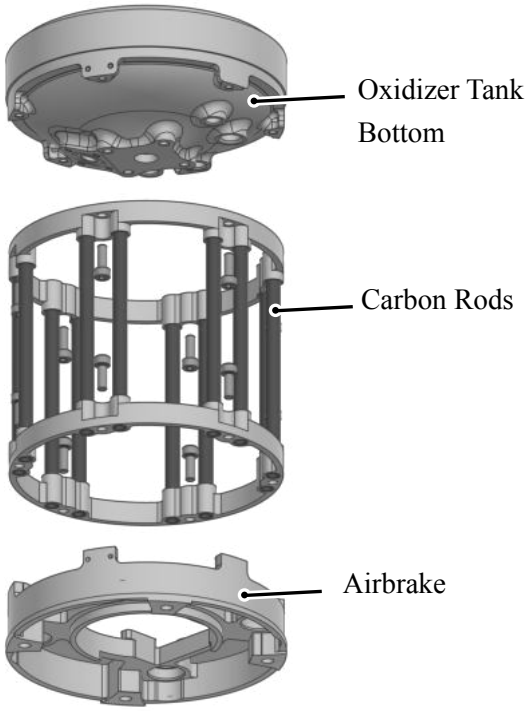

Figure 2.15: Exploded view of the valve bay structure.

2.3.2 Aerodynamics

Nose Cone and Tail Cone

To reduce drag at subsonic speeds, the nose and tail of the rocket were designed using a specific curve from the Haack series, with C = 0. This shape, known as the Von Kármán form, provides the lowest drag for the nose cone at transonic and subsonic speeds. By applying this design to both the front and rear of the rocket, CFD simulations have confirmed that drag is reduced. Furthermore, manufacturing is simplified because the same winding tool can be used for the nose cone and tail cone.
Because the nose cone is wound out of CFRP or GFRP, it is not possible to include the tip in the winding process. Therefore, a thread is placed at the top of the nose cone, where an aluminum tip is inserted, forming the apex of the nose cone.
The curve of the tail cone is shortened to make space for the nozzle. The tail cone is slid over the combustion chamber up to the air brake, where it is secured with radial screws.

Air Brake

This year's rocket ALCEDO will feature a newly developed air brake in order to control the apogee. The system consists of four control flaps that rotate outwards from the rocket's body and, therefore, increase the aerodynamic drag of the vehicle. To ensure the rocket maintains stability, even when the air brake is fully deployed, it has to be mounted behind the center of gravity of the vehicle. Due to the length of the propulsion stack, it is necessary to incorporate the system between the oxidizer tank and the combustion chamber. To do so, the air brake features a unique design, allowing the oxidizer feed pipe to run through the center of the system.

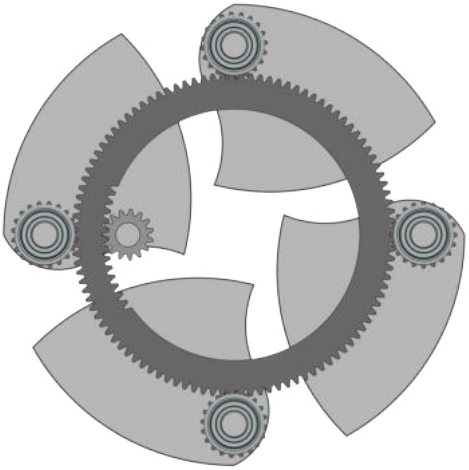

Figure 2.16: The gear mechanism for deploying the air brake.

The air brake is composed of two aluminum plates that serve as the housing for the entire mechanism, a servo motor that actuates the system, and four control flap assemblies that enable the flaps to rotate outward. As shown in figure 2.17 the aluminum base and top plate are screwed together via four M8 bolts holding together the whole system. The servo motor is mounted on the top plate in a position, which ensures maximum space efficiency in the valve bay above. The rotating flap assemblies are enclosed between the top and base plate. The whole air brake system can be assembled and tested without the rest of the rocket.

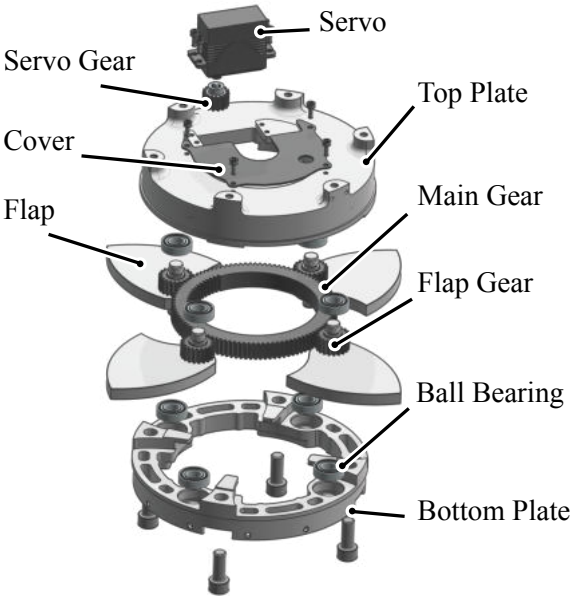

Figure 2.17: Explosion rendering of the Air brake

A gear mechanism is used to transfer the rotational motion from the servo to the flaps. At the core of the mechanism is a ring gear that is externally, as well as partially internally toothed. This specialized gear was manufactured using 3D printing technology, enabling the creation of unique shapes and offering high adaptability. Due to the central feed pipe, the servo is mounted off-center and engages with the internally toothed part of the ring gear. The external teeth engage with four smaller 3D-printed flap gears that are adhered to the shafts.

The control flaps are also mounted on these shafts, which are supported at both ends by ball bearings. This setup allows the flaps to rotate smoothly and absorb the aerodynamic forces acting on the system when deployed. The shape of the control flaps was analyzed in a parameter study. Three aspects were

considered in the design: (1) maximum surface area when fully deployed, (2) sufficient contact between the top and base plates to effectively transfer thrust, and (3) minimum surface area inside the rocket that does not contribute to the functionality when fully deployed. The final form of the flaps ensures all of the criteria above are met effectively. To reduce the weight of the aluminum control surfaces without significantly reducing their rigidity, an isogrid was applied to the underside of the flaps.
The entire system is actuated by the servo motor, which is controlled by the onboard flight computer. To limit the forces acting on the air brake, it will only be actuated during the subsonic part of the coast phase. Simulations show that there is sufficient time to precisely control the apogee of the rocket.
In order to transfer the engine's thrust from the combustion chamber to the air brake and thus the rest of the rocket, a CFRP plate is used. This option was chosen because it is very space-efficient and easy to manufacture.

Fins

The ALCEDO fins are trapezoidal, with the lower base side of the fin adapted to the curve of the tail section. The fins are optimized in their shape to provide enough area as far aft on the rocket as possible and dimensioned in such a way that they guarantee the stability of the rocket at ground-level wind speeds of up to 10 m/s.

To manufacture the fins, 5 pre-preg lay-ups are laminated onto a prefabricated negative fin mold and after curing the two halves are adhesively joined together. A 3D-printed foam core made out of Foaming Light-Weight Acrylonitrile Styrene Acrylate (LW-ASA) fills the inner gap and ensures structural stability at a low weight, while also allowing for a simple manufacturing process. A flange is integrated into the fin shape, which is bonded to the tail section shell with epoxy glue. Aerolastic effects were taken into account when dimensioning the fins by calculating their response to the airflow around them analytically with FinSim.

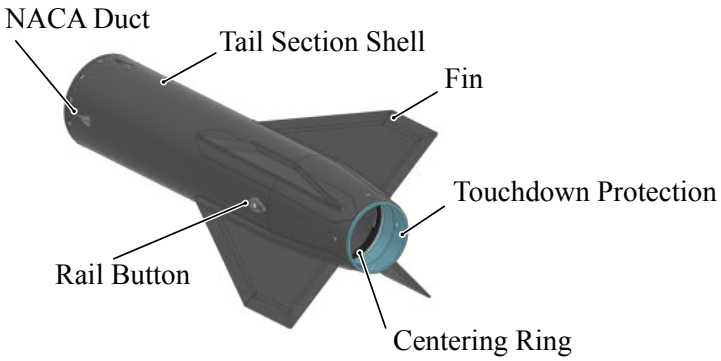

Figure 2.18: Rear view of the fins and tail section.

Tail Section Heat Management

Located at the front of the tail section are four flush inlets. The so-called NACA ducts have a divergent opening contour with a shallow ramp into the rocket. This geometry has the advantage of improved pressure recovery and mass flow into the duct. This is due to the sharp edges of the diverging opening creating two counter-rotating vortices, which displace the slow-moving boundary layer and allow the ingestion of free-stream air. Empirical data from the U.S. National Advisory Committee for Aeronautics (NACA) also show the addition of such ducts does not significantly increase the drag coefficient of the rocket in the transonic regime [**OsephNACASPEEDS**].

The ducts provide cooling airflow around the engine to protect the adhesive joints as well as the rear camera from the heat soak of the engine casing, which can reach temperatures of around 200 °C during flight. The cooling air then flows around the rear heat shield and exits the rocket around the nozzle. The heat shield consists of a 3D-printed shell, with layers of cork and aluminum tape applied to it. It protects

the fins' adhesive joints from the radiant heat from the graphite nozzle, which reaches temperatures of over 1300°C during full duration Hot-Fires. The heat shield additionally protrudes from the rear of the rocket to protect the edge of the composite airframe during touchdown and is thus considered a consumable item.

2.4 Recovery Subsystem

For recovery, a dual deployment system with two separate parachutes is used, as shown in Figure 2.19. At apogee, the first deployment (FD) system separates the nose cone and ejects the drogue parachute to stabilize the rocket at around 28 m/s. The drogue parachute and all its load-bearing components are designed such that a Safety Factor (SF) of 1 can still be guaranteed on an ejection at 200 m/s. The main parachute is deployed at an altitude of 450 m Above Ground Level (AGL) by the second deployment (SD) system to ensure a safe landing at around 9 m/s. The main parachute with its connecting parts is designed to withstand the expected forces at a deployment at 46 m/s with a SF of 2. All ejection mechanisms are physically installed twice. In addition, the electrical ignitors are installed cross-redundantly and the triggering of just one ignitor results in a successful deployment. This means that two ignitors are installed per system. Each flight computer, COTS and SRAD, can trigger one of the ignitors.

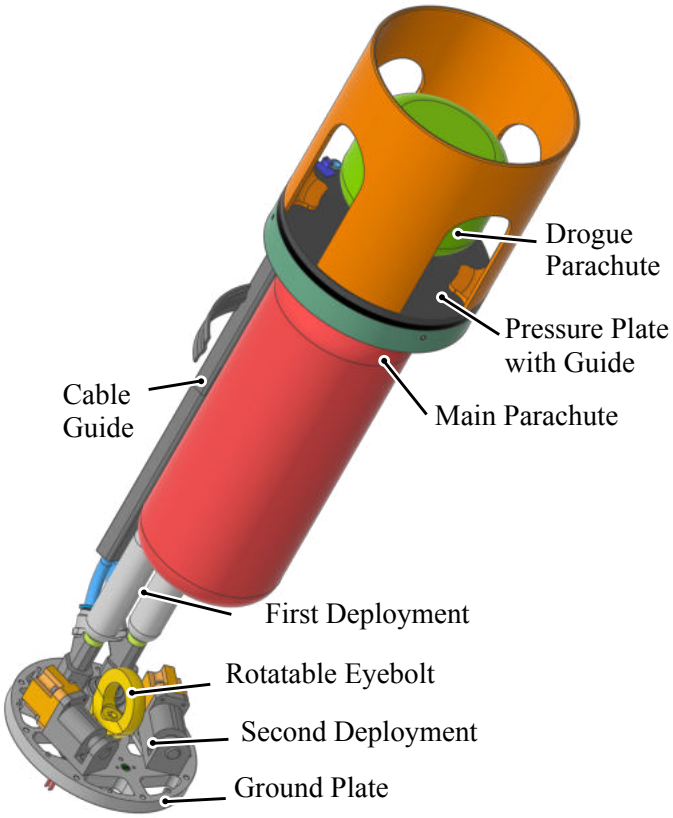

Figure 2.19: Recovery section.

2.4.1 First Deployment

The FD is designed to separate the nose cone from the main rocket body, in further consequence deploying the drogue parachute by pressurizing the pressure chamber. The generated overpressure shears off the M2.5 shear pins, which fix the nose cone to the main rocket body during ascent. Similar to AVES II, this year's FD will have an Ar-capsule instead of a CO_2-capsule, as ice can form inside the tubes when CO_2 escapes, as seen in tests Appendix 28.

First Deployment Design

The first deployment is mounted onto the ground plate, with the Ar-capsule facing up. A 3D-print (TPU filament), called the first deployment pretensioner, between the capsule and the sealing plate, presses onto the thread of the cartridge, which prohibits unscrewing during vibrations. The FD pin lies on a shoulder inside the casing and the Spacer Spring (3D print, TPU filament) prevents premature piercing of the cartridge under vibrations. Right underneath the pin is a PTFE plate that blocks ignition residues clogging up the tread of the pin. Beneath that is the charge cup, encasing the ignitors. The charge cup can be inserted, after the REC-section is fully assembled, from the bottom of the ground plate. To mount the FD to the ground plate, the counter piece screws onto a thread from the casing. A detailed view of the FD is visible in Figure 2.20 and Figure 2.21.

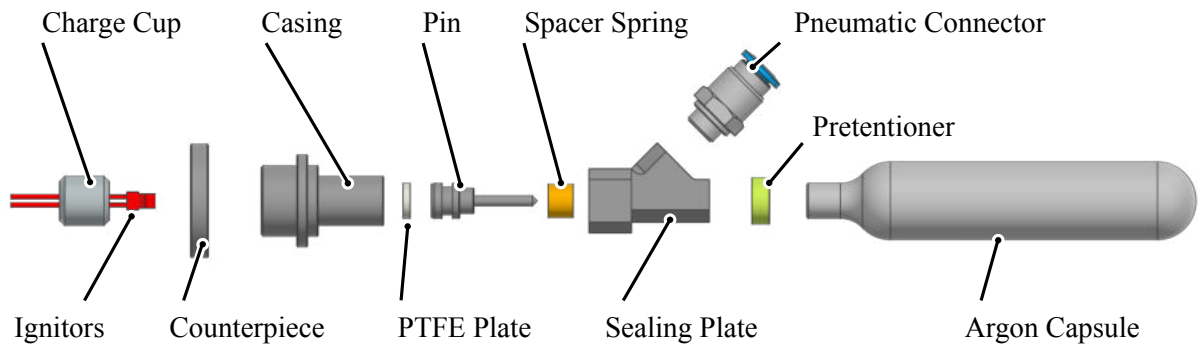

Figure 2.20: Explosion view of FD.

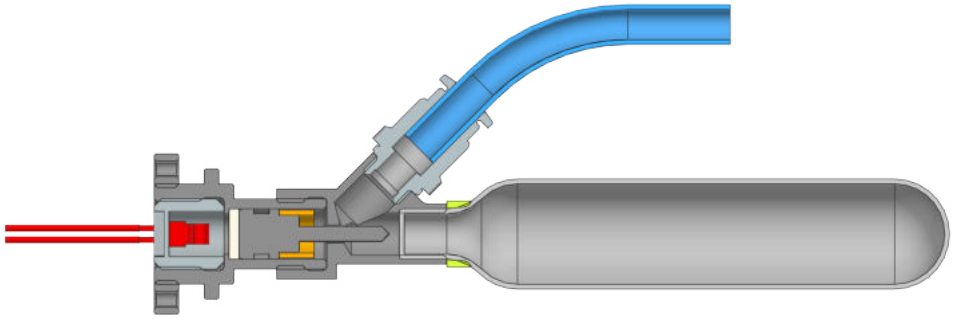

Figure 2.21: Sectional view of the fully assembled FD.

Explanation of the Mechanism

The ignition signal is sent to the ignitor from one of the two flight computers via the interface PCB. The triggered ignitor produces an overpressure in the charge cup. The ignitor alone is strong enough to move the pin, so no further explosive substances, such as NC-powder (Nitrocellulose), are required. In further consequence the pin is accelerated towards the Ar-capsule. The tip of the pin pierces the cartridge and creates a hole. The gas flows via the hole in the sealing plate, the pneumatic connector, and the pressure hose into the pressure chamber.

Pressure Chamber

The pressure chamber is formed at the lower side by the Pressure Plate, at the upper side by the Payload Retainer Plate and the outer boundary is the Coupling Tube. The Pressure Plate Bolt is located in the middle of the Pressure Plate. To prevent tilting during the FD event, a Pressure Plate Guide is attached to the upper side of the plate. The pressure chamber is fully sealed except for the required ventilation hole. The venting hole was taken into account in the calculation and the Safety Factor (SF) is above 2. More detailed information can be found in the calculation under Appendix I.

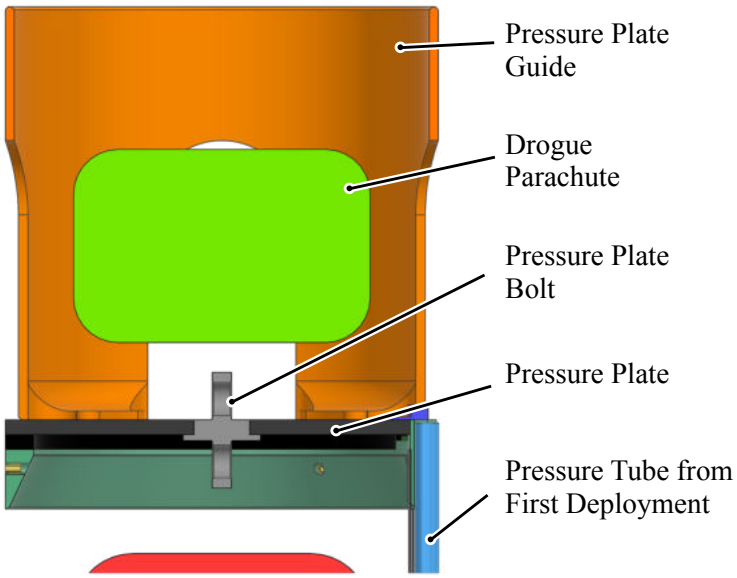

Figure 2.22: Sectional view of the pressure chamber.

Redundancy

Electrical redundancy can be achieved by two independent flight computer (further detailed in Section 2.5.1), each controlling one ignitor per deployment. Mechanical redundancy is achieved by installing two identical deployments. This means that two identical deployments are used with two ignitors each.

Detection

The first deployment detection is designed to determine whether the nose cone has been separated. It consists of a plug that is connected to the pressure plate. The socket is screwed into the pressure chamber ring protection, see Figure 2.23. The continuity of this electric circuit is monitored by the flight computer. When the first deployment is activated, the pressure plate is pulled out which interrupts the circuit.

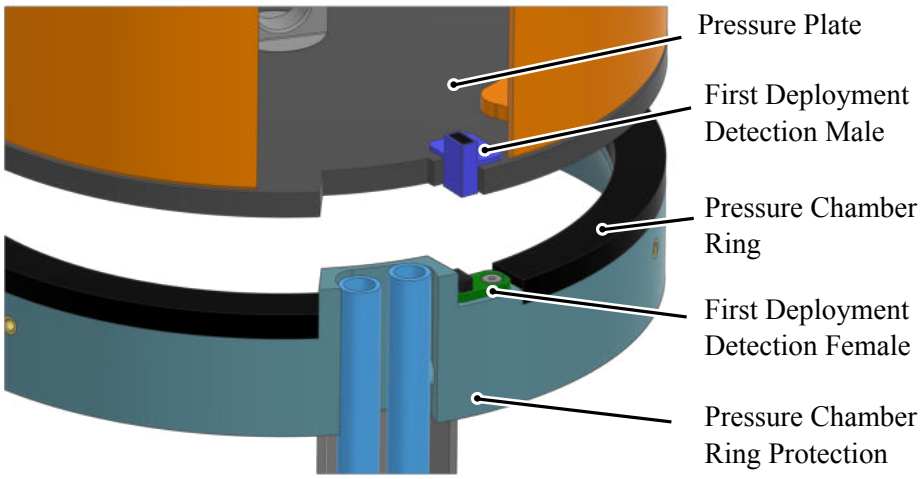

Figure 2.23: View of the pressure chamber with the FD detection.

2.4.2 Second Deployment

The task of the second deployment is to retain the main parachute bag inside the rocket to prevent the opening of the main parachute. As soon as the threshold of 450 m is reached during descent, the second deployment is triggered and allows the main parachute bag to exit the rocket due to the pulling force of the drogue parachute which is attached at the upper side of the parachute bag, as shown in Figure J.5.44.

Second Deployment Design

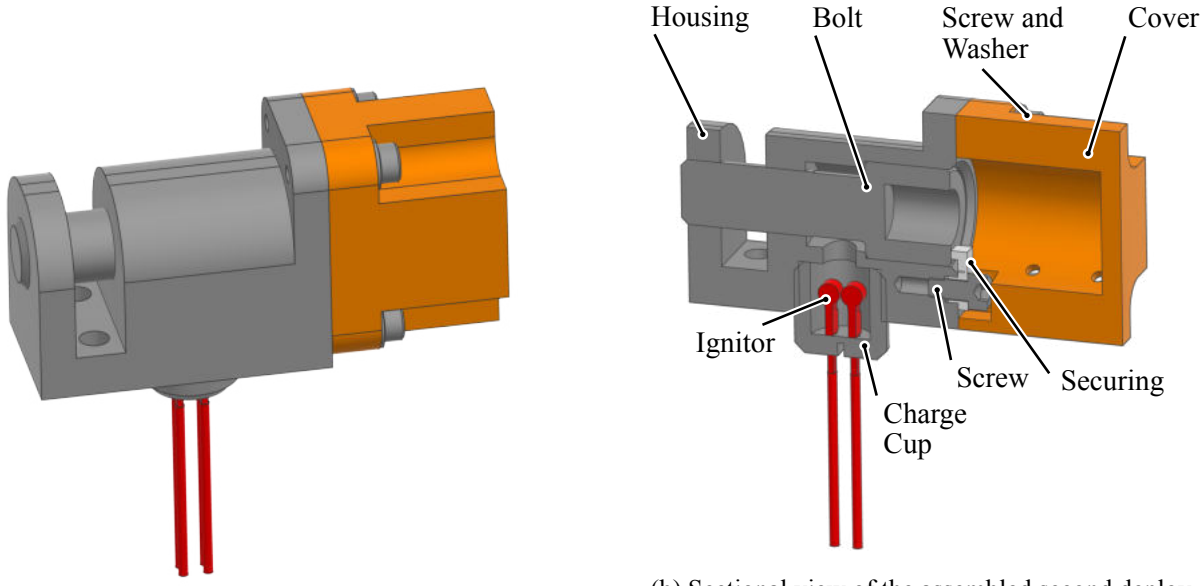

(a) 3D - view of the assembled second deployment.

(b) Sectional view of the assembled second deployment.

Figure 2.24: 3D and sectional view of the SD

.

The housing is secured to the ground plate using two screws. As can be seen in Figure 2.24, the charge cup is located at the bottom of the housing, where the wires are threaded through the ground plate. To prevent the bolt from sliding out prematurely, it is held in place using a securing made out of ASA filament with an intended breaking point. Two ignitors are situated in the charge cup, each capable of moving the bolt from its original position. Ignitors have been chosen as they are easy to insert and use, safe, and reproducible. Four screws are used to mount the housing to the cover (3D printed, TPU), preventing it from deforming and/or bending to either side. The cover confines the bolt and protects the surrounding parts from its potential impact after firing. Made out of a flexible material (TPU), it is capable of withstanding the force of the accelerated bolt even when both ignitors are triggered.

Explanation of the Mechanism

When triggering the ignitor, overpressure is created in the charge cup, thrusting the bolt out of its original position and breaking the securing at the intended breaking point. Thereby, the second deployment connection is released, hence releasing the parachute. The bolt is caught by the cover and confined within the given space.

Redundancy

Electrical redundancy is achieved in the same manner as explained in the FD section. Mechanically the main parachute bag is retained via a cord with two loops that are connected to the second deployments. Triggering one or both deployments leads to the release of the bag.

Detection

The second deployment detection works similarly to the first deployment detection. The continuity is measured and a disruption is detected by the flight computer. In the case of second deployment detection, the plug is connected to the bag via a line (see Figure J.5.43). When the bag is released by the second deployment, the connector is pulled out and the continuity is interrupted (see Figure J.5.44).

2.4.3 Parachute and Lines

Parachute Design

The yellow drogue parachute features a cross-shaped design with a side length of 50 cm, as seen in Figure 2.25a. The shape was selected for its flight stability, which was evaluated in previous projects, where it outperformed elliptical types. The same applies to the used fabric, where Kevlar allows for a stable and durable behavior at high wind speeds. As an estimate for the produced drag, the parachute was tested at various wind speeds (20 m/s, 25 m/s, 30 m/s) and the resulting product of drag coefficient c_w and projected area A is $c_D A = 0.59\,\mathrm{m}^2$. The projected area cannot be assumed to stay constant at different wind speeds, therefore A is also an unknown. The product is shown to behave very stable. With this value, the opening shock can now be calculated. When the Drogue is ejected into an air-stream of 200 m/s, the expected shock force is $F_{Shock,Drogue} = 5236\,\mathrm{N}$. The drogue parachute has a terminal velocity at 450 m AGL of $v_{Max,Drogue} = 28.17\,\mathrm{m/s}$.

(a) Cross shape of the drogue parachute.

(b) Close up of the lashes on the drogue parachute. The outer lashes are sewn over the whole length for stability.

Figure 2.25: Picture of the Drogue parachute and its lash.

The elliptical main parachute consists of ten gores and twenty lines, as seen in Figure 2.26a. The purple and orange colors were chosen to contrast the blue sky and the white clouds. It also stands out from the ground vegetation most prominent in the area to ease the retrieval operations after landing. The main

parachute has a diameter of 2 m. The spill hole at the top is 20 % of its diameter, 40 cm in diameter. Its shroud lines are 1.5 times the diameter, 3 m, and each of them is connected to the parachute on a V-lash, as seen in Figure 2.26b. The deployment of the main parachute was tested in a wind tunnel at 20 m/s, where the lashes and the parachute showed no signs of damage (see Appendix 30). Sensor data from a drop test in Appendix 36 were used to determine the drag area $c_D A = 4.90\,\mathrm{m}^2$. This results in a terminal velocity $v_{Max,Main} = 9.77\,\mathrm{m/s}$ at 450 m AGL. When the main parachute is ejected into an air-stream of 46 m/s, the expected shock force is $F_{Shock,Main} = 864\,\mathrm{N}$.

(a) Elliptical shape of the main parachute.

(b) V-lash on the skirt of the Main parachute.

Figure 2.26: Pictures of the main parachute and its lash.

Bag Design

The design of the parachute bag is based on common rescue parachute bags for paragliding. The bag is closed with four leaves, each having a lug in the middle (see Figure 2.27a). One leaf has an elastic loop which is threaded through the lugs of the other leaves. The loop is held in place with the main shock cord (see Figure 2.27b). To open the bag, the main shock cord has to be placed under tension, which is achieved after the second deployment event. The reliability of the bag staying closed before deployment was tested in the wind tunnel.

(a) The bag is open and has the main parachute with the lines and cords inside.

(b) The bag is held closed by the main shock cord.

Figure 2.27: The pictures show the main bag opened and closed.

System Reliability Measures

An air-porous material was used for the main parachute. This reduces the shock forces and stabilizes the flight. The shock forces are further reduced by the use of a shock absorber during the first deployment and ductile shock cords. A Kevlar sleeve is sewn onto the shock cord to protect it against the scraping of the rocket edges (Figure 2.28b). A thimble provides reinforcement of the connection lines against mechanical parts (Figure 2.28b). To prevent the parachute lines form tangling up, a rotatable carabiner is used. This ensures that the rotating motion of the rocket body and parachute are decoupled (Figure 2.28a).

(a) The rotatable carabiner is used to decouple the spinning of parachute and rocket.

(b) The connection line is reinforced by a metal thimble and a Kevlar sleeve.

Figure 2.28: The close up images show the thimble of a connection line and the rotatable carabiner.

Every part involved in the drogue parachute ejection is calculated to withstand a shock force of 5236 N. This is the force expected at an ejection at wind speeds of 200 m/s. During the main parachute ejection at a wind speed of 46 m/s shock forces of 864 N are expected. All components involved are designed to withstand at least twice that force, see Table A.0.4 and Table A.0.10

Line Management

A detailed schematic of the line management, including the placement of the parachutes and parachute lines, the length of the lines, and all connection points, can be found in Appendix J.5.

2.5 Flight Computer Subsystem

The flight computer subsystem of ALCEDO plays a pivotal role in ensuring successful system operation. Its responsibilities span critical functions, such as controlling actuators in the propulsion system, reading various sensors, managing the deployment of the recovery system, actuating the air brake and valves, and handling telemetry for both data transmission and command reception.

Building on the foundation of the flight computers used in previous projects, this latest iteration integrates several established and reliable features, including an SD card encased in CFRP used as a blackbox, an integrated cooling solution and the powerful STM32 Microcontroller Unit (MCU) at its core. In addition to these proven components, the system incorporates several new developments and optimizations, further enhancing its capabilities.

2.5.1 Recovery Electronics

The primary purpose of the recovery electronics is to reliably actuate the FD and SD of the recovery parachutes. Figure 2.29 provides an overview of the components responsible for these deployments. The CATS Vega was selected as the COTS recovery electronics due to its compact design and versatile programming capabilities for recovery events. Together with the SRAD main flight computer, the two systems provide the necessary redundancy of the recovery deployment. The diagram illustrates the complete cross-redundancy of the system, where each flight computer can trigger the deployment.

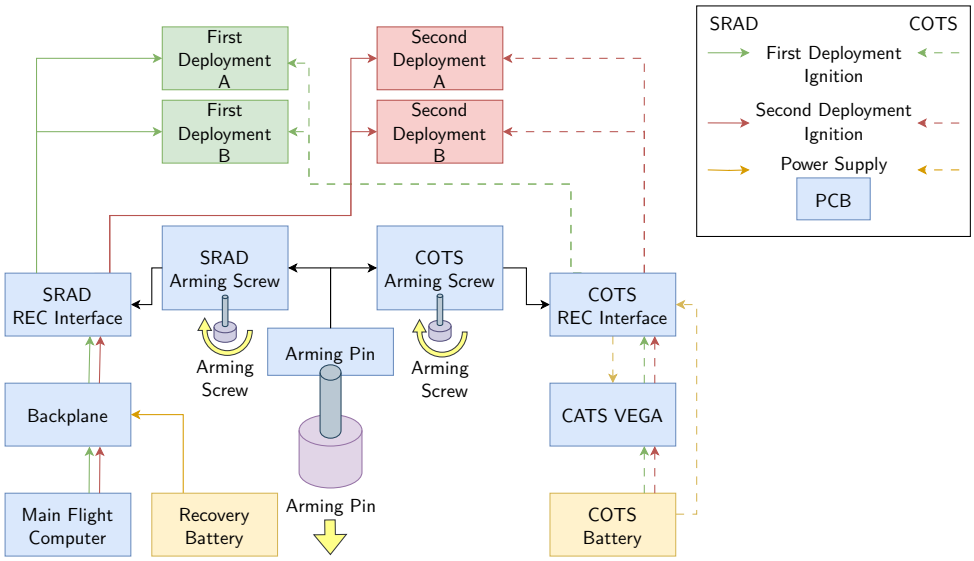

Figure 2.29: Cross redundancy of the recovery system triggered by COTS flight computer and SRAD main flight computer.

To arm both flight computers, operators must secure the two screw switches with a hex key through the designated access holes, then remove the arming pin. The armed status is independently indicated by visible Light Emitting Diodes (LEDs) and audible buzzers for each flight computers.

The recovery and COTS interface PCBs act as passive connectors for the recovery electronics, routing the pyro-channels to terminal blocks for ignitor wire connections. The main flight computer measures ignitor resistance to verify the proper connection of the ignitors and also detects successful deployment of the first and second parachutes via the mission control, ensuring that both the ignitor connections and deployment events are reliably confirmed.

2.5.2 Sensor and Control Nodes CANary

The CANaries are SRAD PCBs that both sample sensors and control actuators while communicating with the flight computer via Controller Area Network (CAN) bus. The eight sensor channels can be configured individually for either thermocouples, pressure, or strain sensors. This approach allows maximum flexibility in later design decisions and a wide range of applications of the same hardware. In the same sense, a CAN bus was chosen for virtually unlimited expansion potential. Each CANary board is equipped with two types of actuator controls: two Pulse-width Modulation (PWM) channels with adjustable voltage supply for servo outputs, and three high-power digital outputs for other types of actuators.

Figure 2.30: The CANary PCB.

2.5.3 Power System

Battery Pack

The primary power system for the rocket is a custom-built battery pack that includes two sections: a 6S (six cells in series) 18650 lithium-ion (Li-ion) battery, which powers the main rocket systems, and a 2S (two cells in series) 18650 Li-ion battery dedicated to the SRAD recovery ignition system. The main battery, with a capacity of 3500 mAh, is designed to support full rocket operations for a minimum of three hours. The battery pack, shown in Figure 2.31, integrates a battery management system to ensure safe and efficient charging of the main battery cells. Additionally, the electrical umbilical cable allows for power supply and battery charging during pad standby to extend operational readiness.

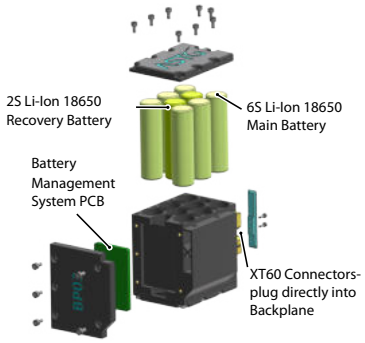

Figure 2.31: The battery pack.

Power Distribution and Management

The power distribution and management system, shown in Figure 2.32, outlines the primary power flow within the rocket, excluding the recovery system. It includes the main battery, internal electrical umbilical PCB, and various subsystems connected via the main power bus on the backplane. It incorporates voltage and current sensors, enabling real-time monitoring of power consumption and battery charging status for both the system and the battery.
This setup ensures reliability by automatically switching between external and internal power sources. During flight, when external power is unavailable, the system seamlessly transitions to the internal battery. The figure also shows the electrical independent connection of the vent valve override, which is discussed further in Section 3.2.2.

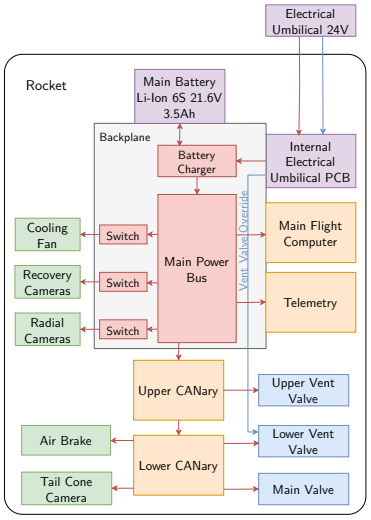

Figure 2.32: Power distribution overview.

2.5.4 Avionics Stack

The avionics stack is the main avionics assembly that includes critical components such as PCBs, batteries, and subsystems like the flight computer, telemetry, and recovery systems. Designed to create a compact and reliable system, the avionics stack reduces internal wiring complexity while ensuring strong performance during flight. This integration allows for efficient testing and easy access before final rocket assembly, as shown in Figure 2.33.

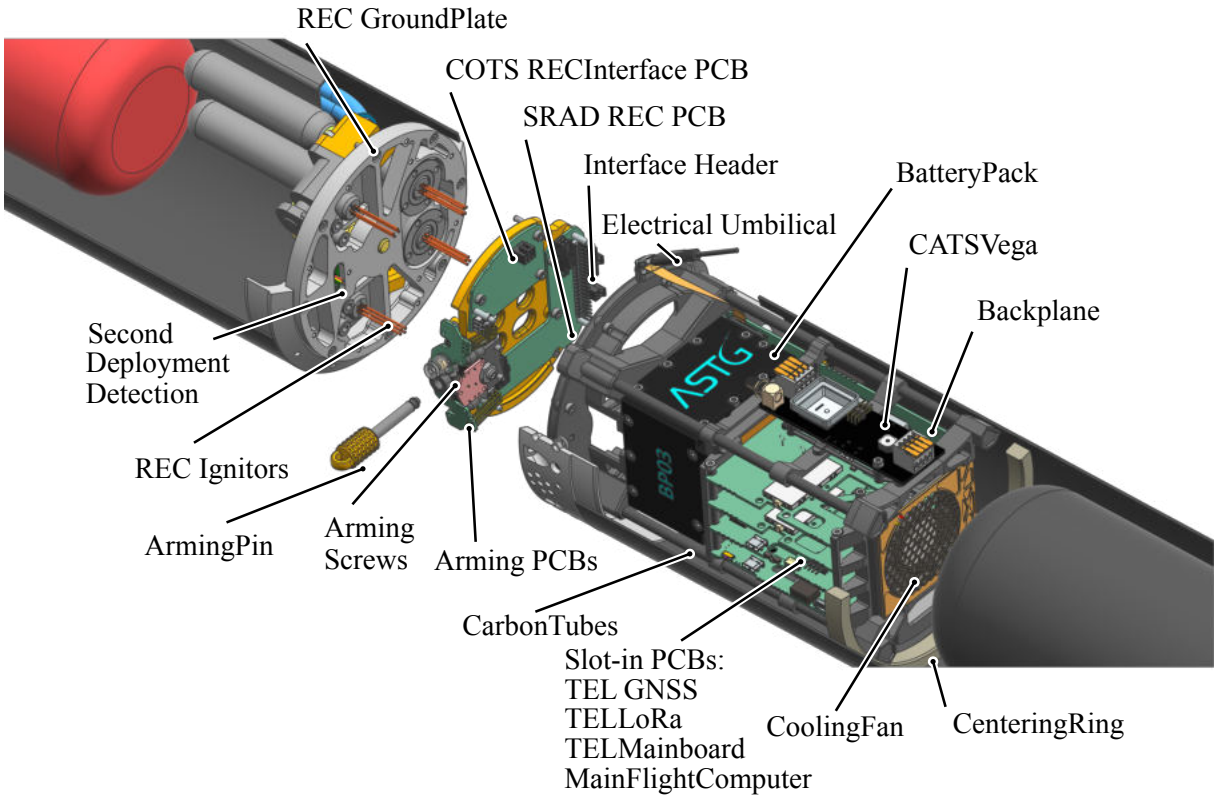

Figure 2.33: Overview of the avionics stack and its components, including the avionics mount.

A key part of the avionics stack, the avionics mount, supports all components securely and interfaces with the recovery system. It holds PCBs, batteries, and cables in place while connecting to the centering ring at the bottom of the structure to prevent lateral movement. The overall system design, depicted in Figure 2.33, ensures that the avionics stack integrates seamlessly with the other subsystems.

The avionics mount is 3d-printed from nylon, reinforced with carbon tubes, and designed with airflow channels for cooling. The backplane is mounted on the avionics mount and serves as the central interconnect for subsystems, supporting standardized form factors for both FLI and TEL PCBs. This design enables easy and flexible swapping of PCBs when testing or replacement is needed due to malfunction. Up to four PCBs can be securely attached to the avionics mount using two bolts, ensuring a stable connection during flight.

As shown in Figure 2.33, the REC interfaces are mounted on the REC ground plate and are responsible for connecting the ignitors. After the ignitors are connected, the avionics stack can be secured to the REC ground plate via the interface header on the backplane and fastened with bolts. During insertion of the avionics stack into the avionics section, the necessary cables are connected. Once fully seated, the avionics stack rests within the centering ring, ensuring stability and minimizing lateral movement.

2.5.5 Main Flight Computer and Backplane

Main Flight Computer

The main flight computer, shown in Figure 2.34, is a critical component of the rocket's avionics system, responsible for data acquisition and system control. Powered by an STM32H745 MCU, it integrates a 3.3 V regulated power supply and features two MS5607 barometers for precise pressure measurements down to 10 mbar, as well as two BMI088 Inertial Measurement Units (IMUs) for accurate inertial sensing. The main flight computer connects directly to the backplane via a Peripheral Component Interconnect Express (PCIe) interface, ensuring reliable communication and power supply, simplifying overall system integration on flight day.

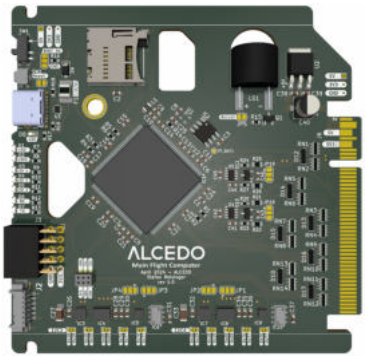

Figure 2.34: Main flight computer.

Backplane

The backplane PCB, illustrated in Figure 2.35, runs throughout the length of the avionics mount and serves as the central interconnect for all components. It features PCIe connectors, battery sockets, and various other connections, which facilitate efficient and organized wiring within the rocket. Additionally, it hosts a combined buck-boost battery charger, the LTC4020, which ensures stable power management. This design minimizes the need for additional cabling and provides a reliable, compact, and easy-to-assemble avionics stack.

Figure 2.35: Backplane.

2.5.6 State Diagram and Software

Operating System

The software for the ALCEDO flight computer is built on a custom SRAD Real-time Operating System (RTOS) known as RavenOS. This RTOS, derived from SmartOS[**Scheipel2022SmartOS:Systems**], is specifically tailored for use in ASTG projects. Developing a custom RTOS allows for system optimization to meet specific hardware and functional requirements, resulting in a significantly smaller codebase and reduced runtime overhead. The primary core of the STM32H745ZIT3 MCU is dedicated to running the main software, while the secondary core is assigned to handle time-critical data management tasks.

Flight Computer Software

The flight computer software is organized into distinct tasks, each dedicated to a specific system functionality. This modular approach facilitates the development of well-structured code that is easily reusable across multiple projects. The benefits of this design are apparent when comparing the state diagram of the flight computer software for the rocket with that of the FS, as shown in Figure 2.36 and Figure 3.3, where several software states are nearly identical.

The various states of the rocket's flight computer software are illustrated in Figure 2.36. These states are categorized into green states, where the rocket is safe to handle, and red states, indicating that the rocket may be filled with fluids. Upon startup or after a reset, the flight computer initializes in the startup state. During the system check state, all components in and around the rocket undergo thorough checks. Once these checks are completed, the starting height and orientation are calibrated in the calibration state.

Following calibration, the rocket enters the green idle state, where it remains until the FS is ready for the Filling State.

During the filling and pre-launch states, the rocket and FS are synchronized, ensuring they remain in the same state and can only progress to the next state simultaneously. Once both flight computer systems are prepared for launch, the software transitions to the ignition state. In this state, the rocket's flight computer awaits the ignition command from the mission control box before initiating the countdown, during which the rocket verifies that all systems are ready for launch.

The countdown can be canceled by flipping both abort switches on the mission control box, which keeps the flight computer in the Ignition State, allowing the countdown to be restarted if necessary. If any unexpected events occur while the rocket is on the ground, the flight computer can be transitioned to the soft abort state. In this state, all actuators, except the engine ignitor, can be controlled by the mission control, ensuring that the rocket can be brought into a safe state.

With the ability to target either 9000 m or 3000 m the flight computer software can be configured into corresponding modes that affect the systems discussed in Section 2.5.6 and Section 2.5.6. The current mode is displayed in the mission control to ensure the correct selection.

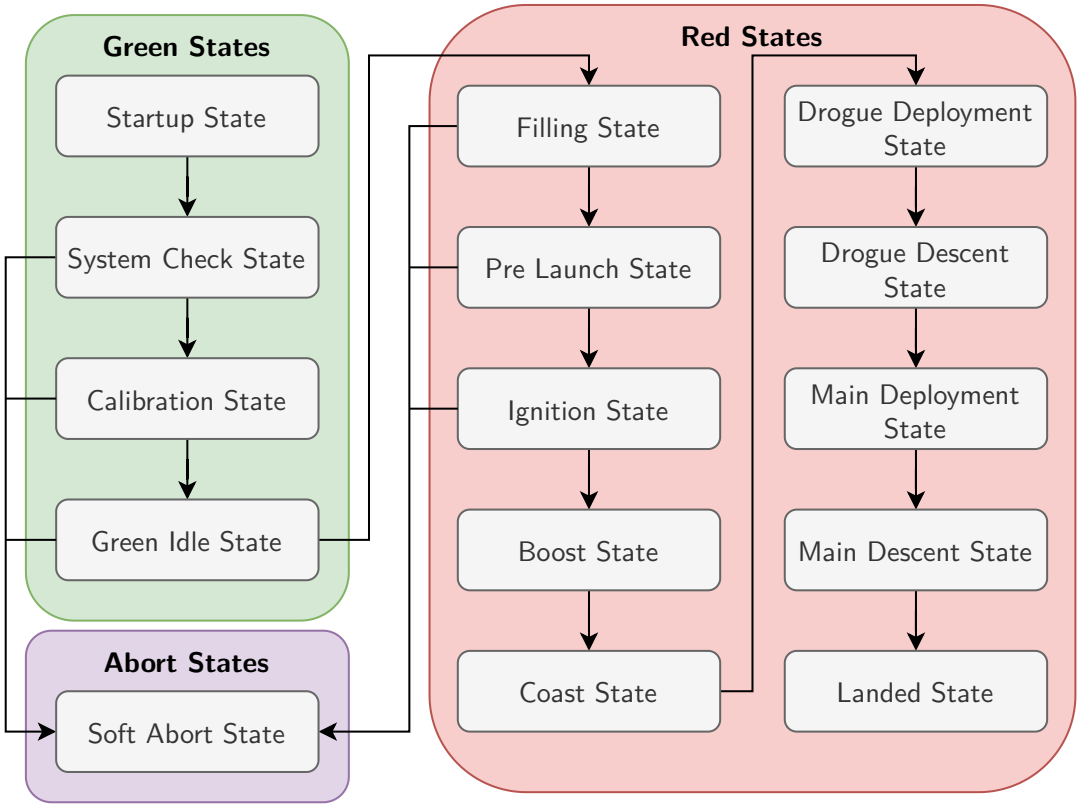

Figure 2.36: State diagram of the SRAD flight computer of the rocket, depicting the different states the flight computer software can be in.

When everything functions as intended and the rocket lifts off, the automatic state detection, as described in Section 2.5.6, takes over. This system advances the rocket through the subsequent states until it reaches the landed state.

Filter for Altitude Calculation

To calculate the height, the barometer and IMU data are processed through a Kalman Filter, enabling sensor fusion and providing predictions in case of sensor failure. To account for the rocket's orientation,

the acceleration data is transformed from body coordinates to Earth coordinates using gyroscope data and quaternions. When the rocket reaches supersonic speeds, the barometer sensors may experience significant fluctuations. To mitigate this effect, the Kalman Filter skips the prediction step above 320 m/s and increases the ratio of measurement to input error, giving greater weight to the acceleration data during this period.

Automatic State Detection

The automatic state detection system is responsible for seamlessly transitioning the rocket from one state to the next during flight. Figure 2.37 illustrates all possible states and the specific conditions required to advance to the subsequent state. Certain states are also assigned a minimum duration to prevent premature transitions caused by sensor noise during critical events such as parachute deployment or engine ignition. Additionally, a maximum duration is enforced to ensure that issues like frozen sensor data do not hinder the progression to the next state. According to the set target height, different predefined durations are chosen. To mitigate anomalies in barometric data caused by supersonic flight, the Kalman Filter is configured to prioritize acceleration data over barometric data. Once subsonic speeds are detected, this weighting is reversed, giving more importance to the barometric data.

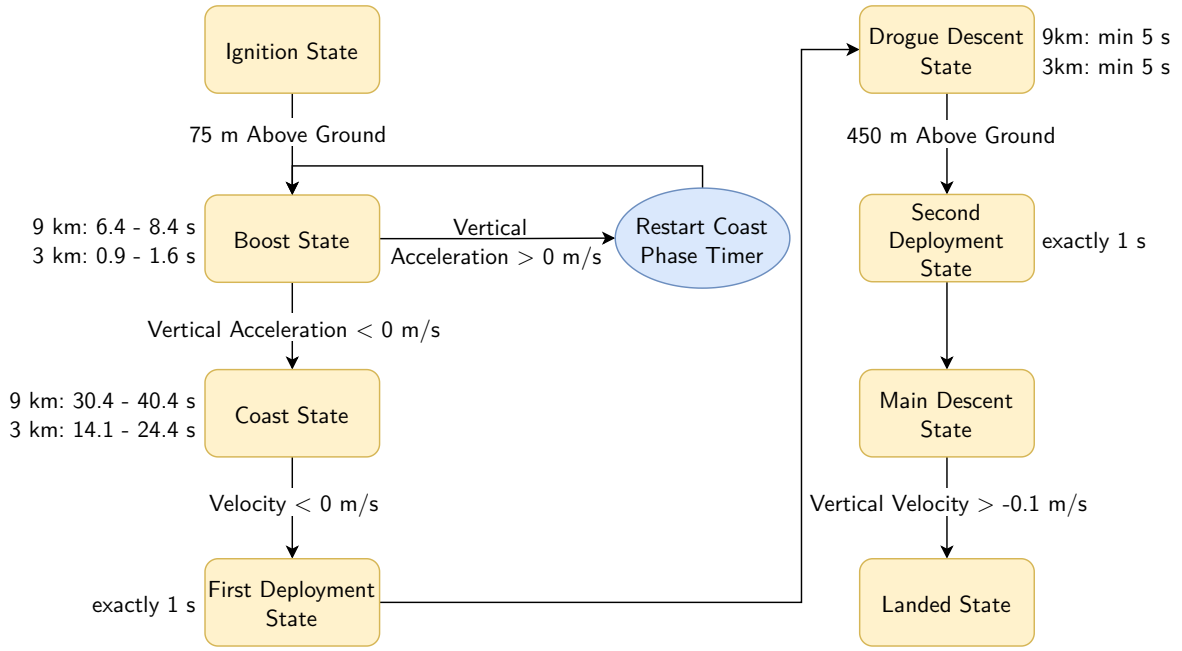

Figure 2.37: Automatic state detection used in the SRAD flight computer, showing the conditions needed for state transitions as well as the minimal and maximal times spent in some states for the different target heights.

Air Brake Actuation

The air brake control software is build utilizing a similar controller as on the AVES II project. There are two major improvements, mainly the air brake will deploy more precisely and slowly using a ramp-up in the control software. This is necessary to improve air brake efficiency and to make sure the air brake will not immediately deploy too fast after air brake software activation, resulting in a more stable flight and braking effect. The second addition is the ability to switch between 9000 m and 3000 m target apogee. The height detection is done by the apogee estimation subsystem, which was built in Matlab and Simulink just like the controller subsystem. The controller is a Proportional Integral (PI) controller and takes the projected apogee, current air brake status, target apogee, and other control values as inputs. The controller then calculates the current ramp-up progress and allows the air brake to deploy accordingly. The goal of

the apogee estimation subsystem is to correctly determine the projected apogee during flight based on current flight data like height, and velocity. The air brake will fully retract at apogee.

2.6 Telemetry Subsystem

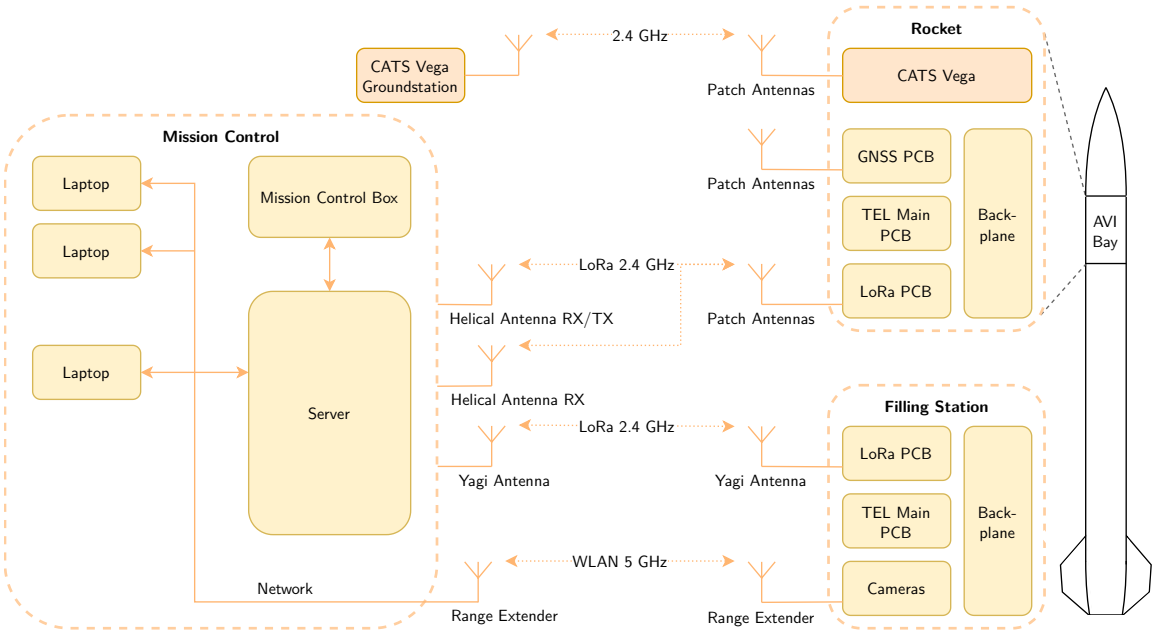

Figure 2.38: Overview of the telemetry system.

The telemetry system's main objective is to wirelessly connect the rocket and the filling station to the mission control in order to control and monitor the status of all system parts remotely.

The connection to the rocket is established using the LoRa protocol. For all RF-communication with the rocket, SRAD patch antennas are used.

There are three PCBs used by the telemetry system, that all fit into the avionics stack using PCIe connectors. All PCBs were designed to be used in the rocket and in the GSE to simplify the design and development process.

2.6.1 Software

The telemetry system consists of three nodes: the rocket, filling station, and mission control, all utilizing virtually the same firmware.

To maximize efficiency, both cores of the dual-core processor are used: one core manages data transmission, while the other is assigned to data processing and other functions, such as interfacing with the GNSS module and gathering hardware data. The communication between these cores and the flight computer is done through a Universal Asynchronous Receiver Transmitter (UART) bus with Direct Memory Access (DMA) for more efficient data transfer.

The system also simulates full-duplex communication over the wireless links by using half-duplex channels with Time-Division Duplexing (TDD), designating distinct timeslots for each node for data sending and receiving.

The approach to reducing protocol overhead is the ASTG Transport Protocol (ATP), a protocol outlining communication among mission control, flight computer, and GSE. Implemented via a C library, ATP focuses on parsing and serializing data packets, managing packet fragmentation, ensuring integrity with a Fletcher16 checksum, and tracking throughput and goodput metrics.

2.6.2 Hardware

The telemetry hardware is split up into three different boards inside the rocket, the TEL main board, LoRa PCB, and GNSS PCB. The same boards are used in the filling station and the mission control. Those PCBs are connected with PCIe connectors onto a backplane. This allows for easy replacement and manufacturing. Rocket, filling station, and mission control each have their own backplane which enable different roles for the PCBs.

Because they proved to be reliable and no modifications or updates were required, the TEL and LoRa PCBs from the previous year's rocket HALCYON were reused.

Main Board

The main board serves as the core of the telemetry system. It houses the primary processor, an RP2040, and provides power to all telemetry PCBs through three Direct Current (DC)-DC converters and a linear regulator. The first two converters supply power to the RF cards, while the third DC-DC converter generates 3.3 V for all digital circuits throughout the telemetry system. The linear regulator also delivers 3.3 V, specifically for powering the analog subsystem.
The analog subsystem contains an Analog-to-Digital Converter (ADC) and two multiplexers. It enables the main board to measure different voltages and currents on it and the RF cards.

Figure 2.39: Main board.

LoRa Board

The LoRa board handles all radio communication within the system. Depending on the set power level and regional regulations, it can function in the 2.4 GHz amateur radio band or the ISM band band. It is equipped with a Semtech SX1280 LoRa transceiver Integrated Circuit (IC) paired with a Skyworks Front End Module (FEM), offering up to 30 dBm output power. This setup includes an integrated RF switch and Low Noise Amplifier (LNA), allowing for two-way communication.
To prevent overheating in high temperatures, a heat sink is affixed to the back of the board. Additionally, the RF section is shielded by a custom-made metal cover, which helps block unwanted signals and minimize electromagnetic interference.

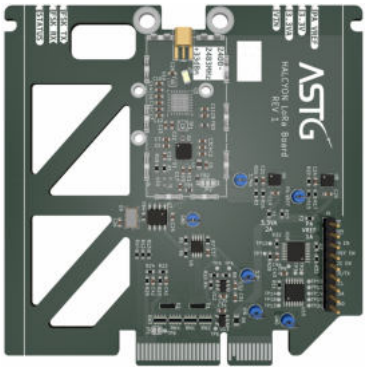

Figure 2.40: LoRa board.

GNSS Board

The GNSS board provides position data to the telemetry system using two TESEO-LIV3R GNSS modules. The two modules are both connected to the accompanying antenna system using a resistive power splitter. Also included on the PCB is a supercapacitor, supplying backup power to the GNSS modules, enabling a much faster position lock after startup. The PCB is designed using the same slot-in form factor as the others and communicates to the main board via the backplane.

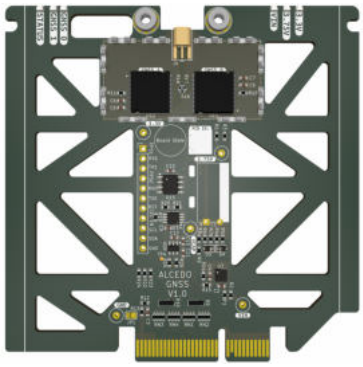

Figure 2.41: GNSS board.

2.6.3 Antennas

In previous years, a 430 MHz radio link was used, which was completely removed due to the large antenna size and the LoRa link (2.4 GHz) working more reliably, with even higher bandwidth and less transmitting power.
Another new feature is the GNSS antenna, consisting of individual patches that are conformally mounted to the body of the rocket.
This year's telemetry system in the rocket utilizes a total of 10 patch antennas on the outside of the rocket's shell.
For the SRAD LoRa link, four patch antennas are mounted in a ring on the outside of the avionics shell. In addition to the SRAD LoRa antennas, two SRAD GNSS patch antennas are used for receiving the GNSS signal for both the SRAD GNSS system and the CATS Vega.
All antennas are mounted on the outside of the carbon tube, with antenna splitters placed on the inside. These are connected to the avionics stack using cables. The removal of the internal monopole antennas also reduces the length of the rocket and makes it possible for the avionics shell to be made of carbon.

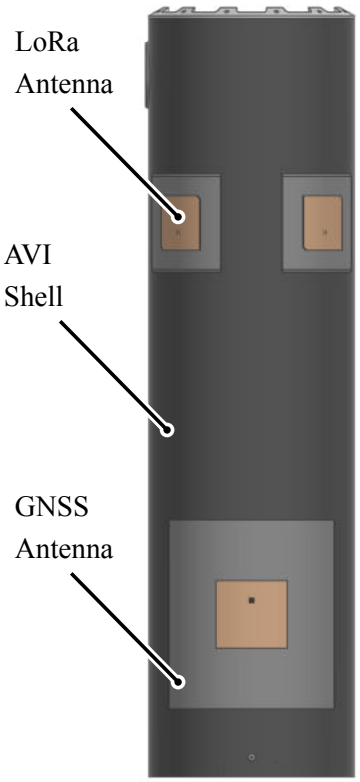

Figure 2.42: Patch antennas and placement on the avionics shell.

2.4 GHz Antenna System

For the patch ring, four identical Right-Hand Circular Polarized (RHCP) patch antennas are used. Each patch has a gain of 3 dB. When combined they sum up to a uniform Fairfield pattern of 0 dB. Four directed patches are combined in a circle to accomplish uniform radiation. Due to this design weight and space are reduced.
To combine the four patches, multiple Wilkinson power dividers and combiners are used. Firstly two patches that are next to each other are combined using the antenna splitter, the two resulting leads are then combined via the core splitter to form a single feeding point.

GNSS Antenna System

In previous rockets, GNSS reception was suboptimal due to unfavorable antenna placement inside the rocket, with each GNSS module having only one antenna. To address this, two patch antennas are now placed on opposite sides of the rocket's shell, providing full sky coverage to improve signal reception. The signals from both antennas are amplified by two LNAs, combined via a Wilkinson power combiner, and then redistributed via a Wilkinson power splitter. One signal path is directed to the telemetry hardware, while the other is routed to the CATS Vega flight computer.
The splitting and redistribution enable both endpoints to achieve full-sky visibility, a significant improvement over last year's design. The patch antennas have a center frequency of 1575 MHz and are RHCP. Due to their larger size, only two patch antennas are used, conformally mounted onto the rocket's outer carbon body.

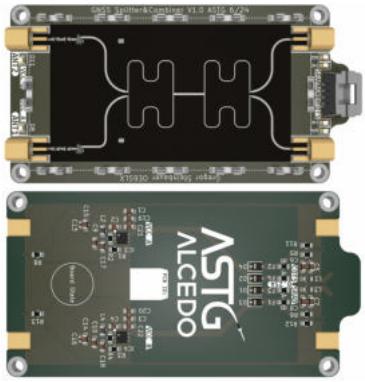

Figure 2.43: GNSS splitter.

2.7 Payload Subsystem

ALCEDO is designed to carry two 1U CubeSats and the DADS up to 9000 m. One of the CubeSats was designed and built by a team of high school students, one was built as a Bachelor's thesis and one is a demonstrator for the REXUS/BEXUS mission, which has become the second large project of ASTG.

2.7.1 Demonstrator Attitude Determination System (DADS)

DADS is a prototype to design, test, and validate the attitude determination system. This system is intended to be part of the REXUS/BEXUS mission APEX which is an additional project of the ASTG. DADS aims to determine the position of the rocket relative to the sun. The system consists of four sun sensors on the outside of nose cone, three high-precision gyroscopes, one three-axis magnetometer, a three-axis IMU as well as the necessary electronics to collect all this data.

(a) DADS main PCB

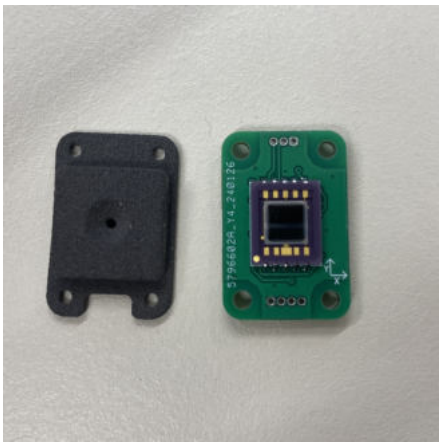

(b) Sun Sensor and Cover

Figure 2.44: Hardware of DADS in the Nosecone.

The batteries are stored in a CubeSat while the PCB and the sensors are directly integrated into the nose cone. This is because the sun sensors must be placed on the outside of the rocket.

2.7.2 Colibri

The Colibri Cubesat is the spin-stabilized camera placed in the lowest CubeSat position to record the rocket's descent. During the descent, the rocket hangs on a single tether under the parachute and spins freely, so to get a clean film the camera has to counteract this spin. This is the mission of the Colibri CubeSat. It consists of a camera mounted on a motor, which is controlled by a MCU that measures the spin and turns the camera to counteract it.

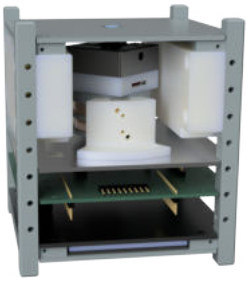

Figure 2.45: Rendering of the Colibri

2.7.3 APD - ALCEDO Payload Development

APD, or Alcedo Payload Development, is a team of four students from HTL Pinkafeld. They designed and developed a CubeSat to measure the muons in cosmic radiation during the rocket's flight. Afterward, the collected data will be visualized. To achieve their goal, the students used a Raspberry Pi 3B with a custom plug-on board by MuonPI, which is responsible for measuring the muons and the corresponding timestamps. The MuonPI has an integrated silicon photo-multiplier to detect the light emitted by a plastic scintillator if excited by a muon. The measurement unit is powered by Samsung INR18650-30 Li-Ion power cells.

Figure 2.46: Picture of the APD

3 Ground Support Equipment System Architecture

3.1 Filling Station

3.1.1 Fluid Architecture

The fluid architecture of the FS, depicted in Figure 3.1, consists of two main lines. One for the N_2O and the other one for the N_2, the pressurizing gas. On one side, they are connected to the fluid bottles, and on the other to the umbilical connection. The oxidizer line features two oxidizer fill valves, manual oxidizer fill valves, and manual vent valves for both oxidizer bottles. Also, the pressure and temperature are monitored in both oxidizer lines. After the servo-actuated oxidizer fill valves a pressure sensor, a temperature sensor, and a solenoid vent valve are located. The vent valve facilitates the depressurizing of the line for safe disconnection of the QD. The oxidizer bottles have a heat sleeve mounted, which is only used if the pressure gets too low for tanking. This has never occurred in the testing campaign, but it is still mounted as a precaution and additionally serves as an insulation for the oxidizer bottle. The outside temperature of the bottles is monitored in two locations to further increase the knowledge of the current state of the system. The pressurizing line also has two connections to the N_2 bottles. Both feature pressure sensors, manual vent valves, and solenoid fill valves. Check valves prevent the unwanted flow of pressurizing gas back into the bottles as the solenoid valves allow for backflow. After the N_2 fill valves a pressure sensor, a solenoid vent valve, a filter, and the connection to the compressor are placed. The compressor is connected with a check valve in between and is not connected to any gas bottle, which means in case the compressor is needed, the rocket is pressurized with ambient air. This is not a problem as early tests were conducted with air as pressurizing gas instead of nitrogen. The solenoid vent valve again is used for depressurizing the line to disconnect the QD.

3.1.2 Electronics Architecture

The FS system operates with a 400 V/16 A main power supply and a 24 V/6 A power supply for the control electronics. Sensor readouts and actuator controls are managed via CANaries, which are connected to a flight computer housed within the electrical cabinet. This flight computer features its own telemetry link to the mission control. By using the same hardware as the rocket, large portions of the code base can be reused, significantly reducing the development and testing time for additional PCBs. The cabinet door is equipped with indicator lamps that display the current state of the system, while additional switches and buttons provide manual overrides for critical functions, such as vent valves and main flight computer reset.

To ensure reliable operation, sensor readouts are separated from high-power actuators. The CANaries are placed in dedicated electrical cabinets, and sensor cables are kept as short and shielded as possible. Additionally, the main power consumers, including the oxidizer bottle heating and compressor, are connected to different phases than the control circuitry, further reducing potential interference.

3.1.3 Safety Precautions

To safeguard against electrical shock and equipment damage, the FS system incorporates multiple safety devices, such as the main load break switch, overload fuses, residual current device, and circuit breakers. Emergency stop switches are installed at both the FS and the safety control box, allowing for the deactivation

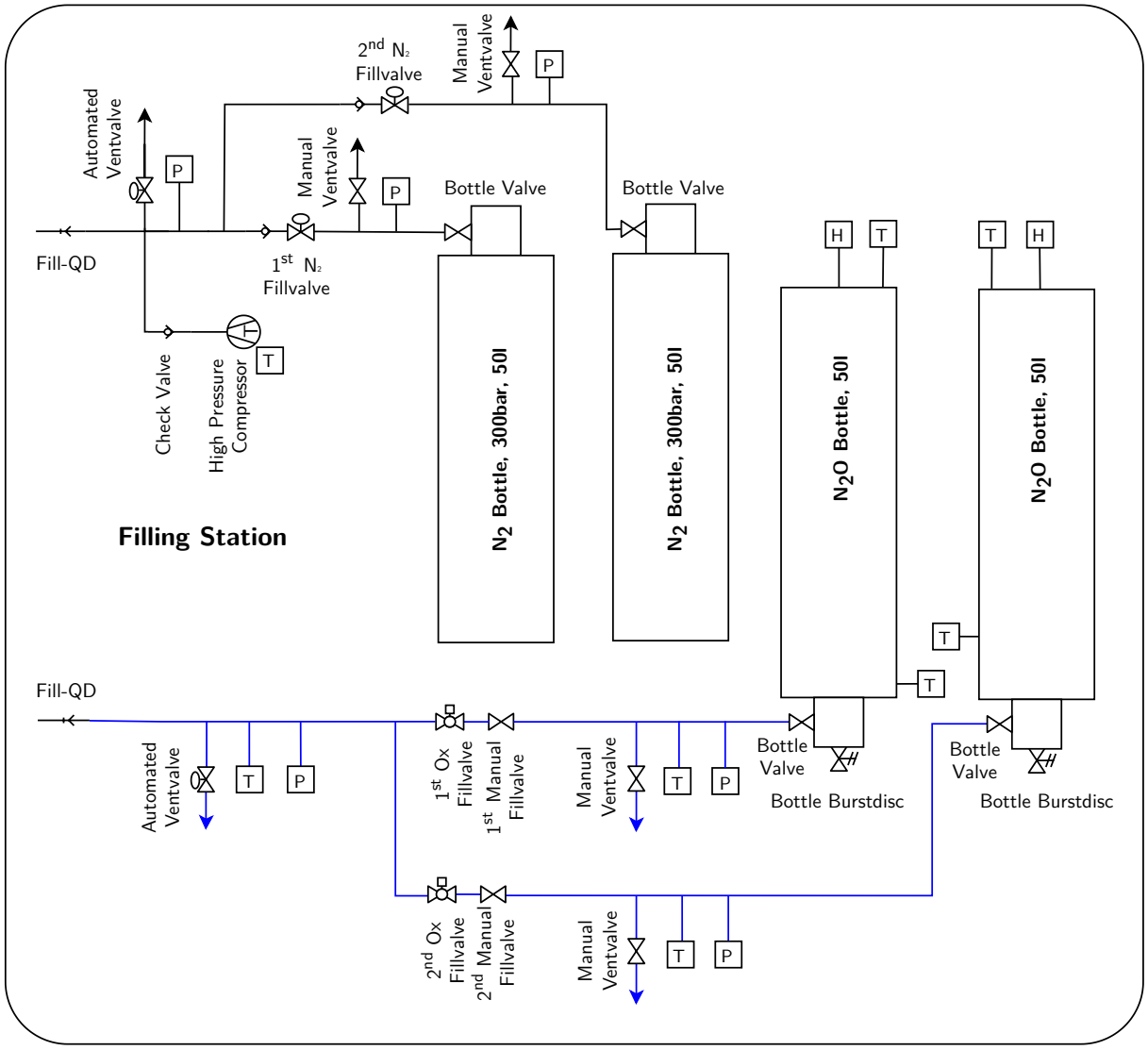

Figure 3.1: Fluid diagram of the FS.

of all high-power components while maintaining power to the control circuitry. Alongside a 24 V lead-acid backup battery, this setup ensures continuous sensor readouts, enabling constant monitoring of the fluid system's status and preventing potentially hazardous conditions from going unnoticed.

All fluid lines connected to the gas bottles can be vented with manual vent valves. This allows the launch rail operator to secure the FS after launch or launch abort. To restrict unwanted flow of pressurizing gas check valves are installed in both lines of the gas bottles and the compressor. In the oxidizer line, manual fill valves are used to improve safety. The launch rail operator opens these valves only after all tasks at the rocket and FS have been completed. This ensures that no personnel needs to go near the ground support equipment once the procedure is underway, keeping personnel out of potentially dangerous areas.

The ignition signal path, shown in Figure 3.2, originates from within the rocket to achieve precise synchronization between ignition and main valve operation. The safety control box, located more than 15 m from the launch rail, manages the automatic control of valves, houses the safety interlock for engine ignition, and provides the interface for ignitor connections.

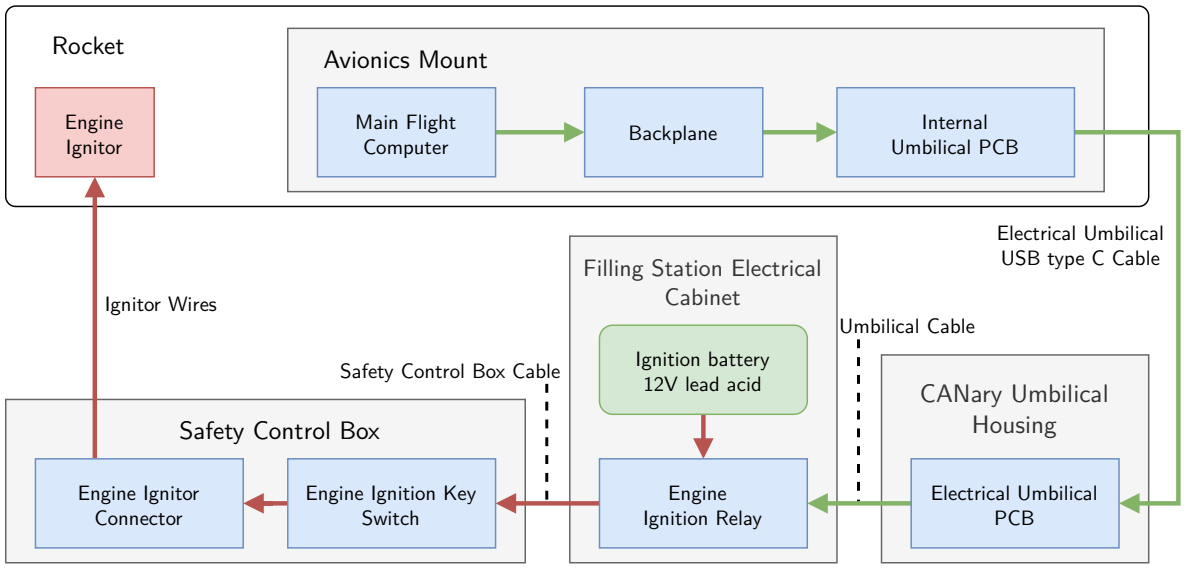

Figure 3.2: Schematic diagram of ignition electronics.

The ignition signal is sent from the mission control box, which includes safety mechanisms for secure actuation. Both the key switch and push button have independent switches connected to separate digital inputs and are also connected in series to an additional input. The software only allows the ignition signal to be sent when all inputs show the correct states. The main flight computer will trigger ignition only when it is in the correct state.

3.1.4 State Diagram and Software

As discussed in Section 2.5.6, the FS uses the same RTOS and general software architecture as the rocket's main flight computer, with much of the code shared between the two systems and only minor adjustments for the four green states. The main difference is the addition of a yellow state, referred to as the propellant preparation state. In this state, the FS operates independently from the rocket, allowing for fluid preparations during tanking, during which certain bottles may be opened, limiting access to specialist personnel only.

Once the rocket is positioned on the launch rail, it can command the FS to transition to the filling state and then to the pre-launch state. After receiving the ignition command and starting the countdown, the rocket's

main flight computer signals the FS to enter the post-launch state, where all valves can be actuated to bring the FS into a safe condition after launch. Additionally, the FS includes the same soft abort state as the rocket, which can be activated via the mission control software, allowing full actuation to handle any potential scenario.

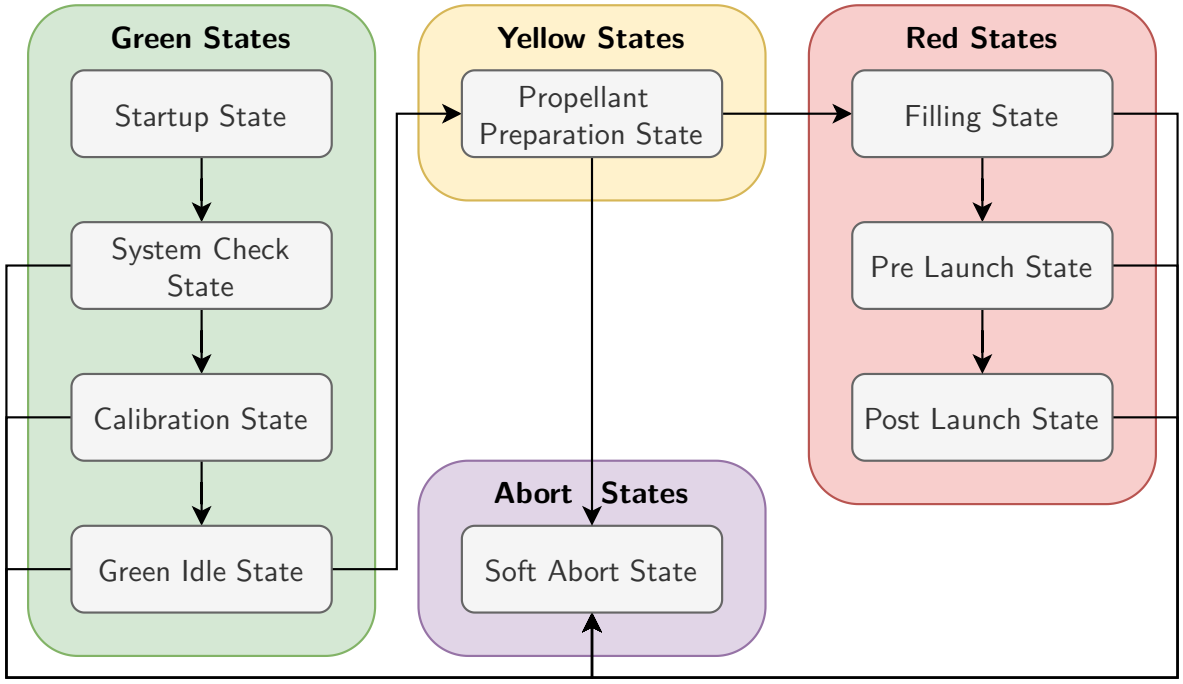

Figure 3.3: State diagram of the FS, depicting the different states the software can be in.

For actuator safety, the FS follows the same safety protocols as the rocket software, as detailed in Table J.3.2. This table provides a comprehensive list of all actuators and their corresponding states in the FS.

3.2 Umbilical Connections

3.2.1 Fluid Umbilicals

The primary role of the fluid umbilicals is to detach the fluid lines of the filling station from the rocket after the fueling and pressurizing processes are completed. The oxidizer and pressurant QD are attached to separate umbilical arms to be able to disconnect them separately at different times during the tanking procedure. This separation is carried out by two servo motors working in parallel to release the fluid QD, which allows the spring-loaded umbilical arm to swing back 180° to get out of the way of the rocket and exhaust stream during launch. The secondary role of the umbilical arm is to pull the insulation clear of the oxidizer tank while swinging back. The two servos are mounted on a linear rail to provide a straight detachment motion for the QD. To disconnect the QD, the servos rotate a custom 3D printed part in the shape of a logarithmic spiral, pushing a plate, which is mounted to the umbilical arm, against the rocket. This action pushes the umbilical arm away from the rocket and disconnects the QD. Both servos operate in parallel to ensure even force distribution; however, testing showed that one of the servos alone is also sufficient to disconnect the system, providing redundancy.

If, in any case, both servos fail to release the umbilical arm, a steel wire is attached to the system, which can be pulled to manually disconnect the QD. The whole QD system is attached to the umbilical arm

with two plates featuring long holes and adjustable screws to provide fine adjustment possibilities while attaching the QD to the rocket.

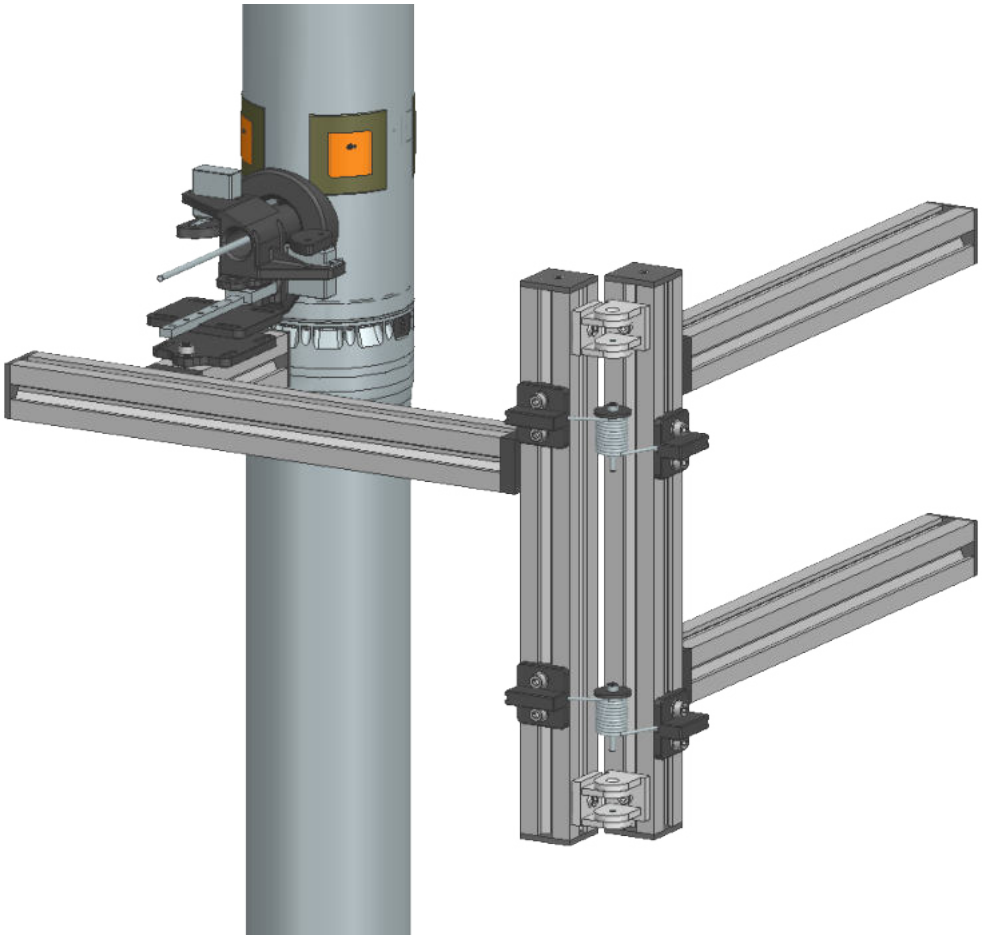

Figure 3.4: Depicted is one fluid umbilical arm that connects the filling station to the rocket and allows for remote disconnection.

3.2.2 Electrical Umbilical

The electrical umbilical functions as a wired connection between the rocket and the GSE while the rocket is on the launch rail. It utilizes a Type-C Universal Serial Bus (USB) cable due to its compact connectors and high power rating of 240 W. The connector on the launch vehicle is situated at the top of the oxidizer tank, angled downwards to allow for automatic unplugging during the acceleration phase along the launch rail.

One of the primary functions of the umbilical is to supply auxiliary power to the rocket, keeping the onboard battery pack charged until lift-off. In addition to power delivery, the cable carries several critical signals: the ignition signal, two-way reset signals, a vent valve override, and a CAN bus signal used for debugging, testing, and communication in case of telemetry issues. The reset lines allow for remote resetting of the rocket using the FS and vice versa. The vent valve override enables actuation of the lower vent valve from a safe distance in case the rocket's electronics become unresponsive as shown in Figure 2.32, ensuring the system can be brought to a safe state. safe state as On the ground side, the electrical umbilical connects to a small electrical cabinet mounted at the back of the launch rail. This cabinet houses a CANary, which controls the fluid umbilical servos and reads sensor data from the wind speed sensor and the rocket weight measurement system.

3.3 Mission Control

Figure 3.5: Mission control setup, antennas are not visible.

The mission control consists of hardware and software designed to monitor and control all systems remotely. It establishes LoRa links to both the rocket and the filling station as its main communication line. The mission control's usual setup is seen in Figure 3.5.

The mission control flight case rack houses the telemetry PCBs, a server for hosting multiple software applications, and network equipment. The mission control box is connected to the flight case rack by a custom connector and provides a physical user interface, containing switches like the ignition button and ignition key switch, as well as critical indicator LEDs.

All controls and any data are accessible through the mission control server using laptops over a Wireless Local Area Network (WLAN) connection, or a wired Local Area Network (LAN) as a fallback.

3.3.1 Mission Control Hardware

The mission control uses a flight case rack to house its main components, allowing for easy transportation and quick setup time. The rack contains the telemetry hardware: the mission control backplane along with a telemetry main board and 3 LoRa PCBs for handling the RF communication. It also contains the server hosting various software, along with a network switch and a WLAN router for access to the mission control network.

To ensure a safe operation even during a power outage, there is an Uninterruptible Power Supply (UPS) that can temporarily supply power to critical systems. Furthermore, ventilation is provided by fans that pull air in through a car Heating, Ventilation, Air Conditioning (HVAC) filter. This creates modest positive pressure inside the flight case and ensures a clean environment.

The mission control box is connected to the flight case rack with a custom Harting connector that contains USB, Ethernet, HDMI, 230 V, 24 V, and digital control signals. The box itself contains four 230 V outlets to connect monitors and laptops, a dimmable power supply for the indicator LEDs, and the mission control Input/Output (I/O) board used to control the indicators and read the switches. The mission control box contains the ignition button, the ignition arming key switch, a vent valve override switch, and several indicator lights for arming, ignition, and the telemetry system status.

Mission Control Backplane

The mission control backplane connects three LoRa PCBs to a telemetry main board and provides digital inputs and outputs to control and monitor different peripherals. Furthermore, it connects to the mission control I/O board via an Inter-Integrated Circuit (I2C) bus to provide a physical interface to the user and the 24 V power supply in the mission control rack.

Mission Control I/O Board

The mission control I/O board is an I2C I/O expander board supporting 16 inputs with double redundancy and 16 outputs.

It is connected to a mission control via an umbilical supplying 24 V power and 12 V logic-level I2C capable of delivering signal up to 100 m.

It is also outfitted with 5 V/2 A and 3.3 V/1 A power supplies to drive the I/O chips and an optional I2C display.

Figure 3.6: Mission control I/O PCB.

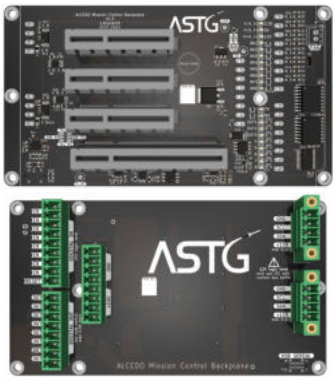

Figure 3.7: Mission control backplane.

3.3.2 Mission Control Software

The mission control features a web-based user interface hosted on the mission control server. This architecture allows multiple clients to connect to the server using a web browser over a standard WLAN network, which enables operators and observers to work independently by using their laptops.

Grafana is utilized together with a custom Vue.js frontend application for data visualization and command execution. These interfaces are supported by a Python backend application and a PostgreSQL database, with the entire system being dockerized to allow rapid setup and reproducibility.

The Python backend application handles reading and writing ATP packets to/from a UART USB device and stores the data in a PostgreSQL database. Grafana accesses the data directly from PostgreSQL and presents it to the user. Command execution is managed through the Vue.js frontend application, which includes specialized Scalable Vector Graphics (SVG) to highlight critical data. It communicates with the Python backend application via a GraphQL Hypertext Transfer Protocol (HTTP) Application Programming Interface (API).

Furthermore, the mission control network includes a WLAN bridge to include Internet Protocol (IP) cameras at the filling station, providing visual confirmation during the tanking process.

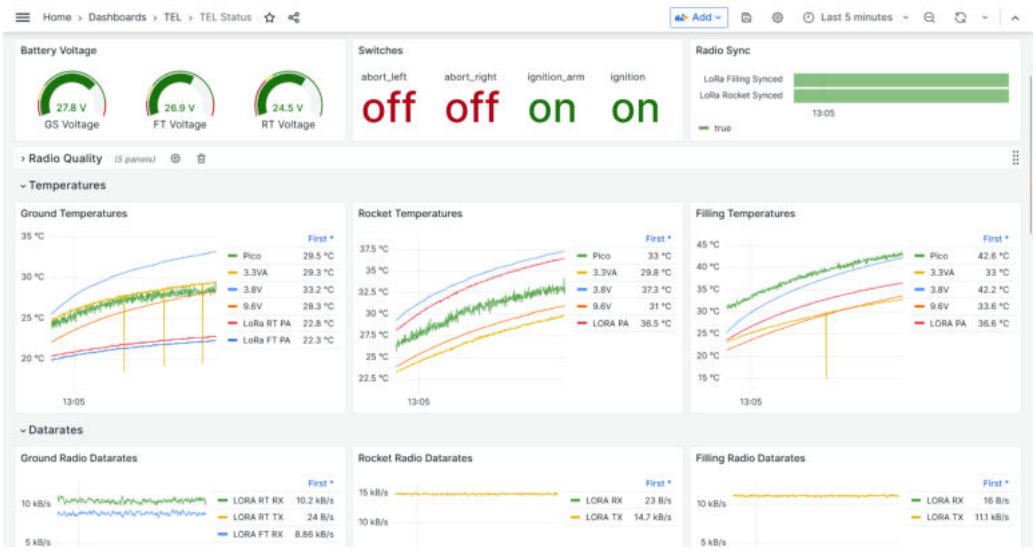

(a) Grafana dashboard with data.

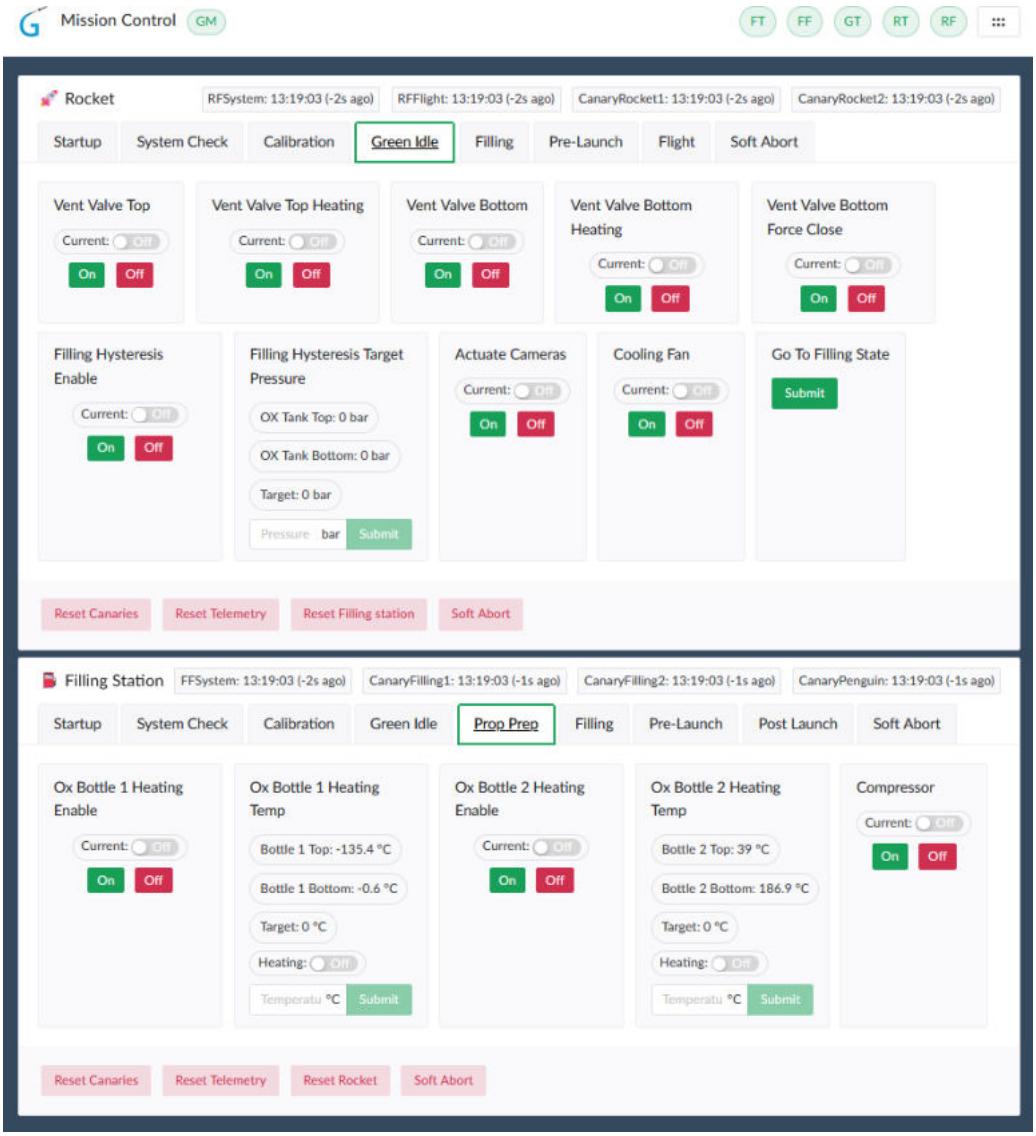

(b) Mission control panel for controlling actuators.

Figure 3.8: Overview of applications hosted on the mission control server.

3.3.3 Antennas

Two helical antennas are used on the ground to ensure a safe connection with the rocket, no matter the attitude. Both use a right-hand polarized signal, the same rotation as the rocket's patch antennas, so the relative position to the rocket does not matter.

One of the antennas, with a dispersion of 42°, is used for a bidirectional connection. The second, with 30° only, is only used to receive data, because it integrates an LNA close to the antenna to improve performance. Both are moved simultaneously by hand to track the rocket. For the LoRa connection to the filling station a stationarily mounted COTS Yagi antenna will be used.

4 Mission Concept of Operations Overview

To achieve a nominal flight of ALCEDO, the following mission concept of operations table was developed. It outlines the necessary procedures and operations crucial to the success of the mission. Starting from arrival at the launch site and includes preparations for the launch vehicle, launch rail, mission control, and FS. The mission is divided into four main phases: the pre-flight handling, the tanking procedure phase, the flight itself, and the post-flight phase.

Table 4.1: Tabulated concept of operations.

Mission/ Operational Phase		Appr. Time (Start)	Phase End	Assembly Tent Team	Mission Control Team	Launch Rail Team	Recovery Team
Storage & Transport		T-7d	Arrival at the launch site	Parts are stored in boxes The propulsion stack is preassembled with the ignitor installed and shunted The avionics bay is preassembled The recovery subsystem is preassembled	The mission control monitors and parts are stored in boxes	The launch rail is disassembled	
Pre-flight - handling	Assembly	T-3h	The rocket is assembled and brought to the launch rail	Final assembly of the recovery subsystem Final assembly of the avionics subsystem Visual inspection of the preassembled propulsion stack Final test actuation of the flight hardware Payloads are switched on Integration of all subsystems into the rocket	Setup of the mission control Establish connection with the filling station and its cameras Establish connection with the rocket Report first sensor data of the filling station	Setup the launch rail Setup the filling station and its antennas Install the N2O and N2 bottles Purge the filling system	
		T-1h	The specialist personnel leaves the launch pad		Final checks of the filling station	Mount rocket to the launch rail Connect all umbilical connections Final checks of the filling station Arm rocket, open manual N2O valve and connect ignition	Prepare for the recovery of the rocket
Tanking		T-30 min	The rocket is fully tanked, pressurized and the umbilicals are disconnected		Controlling the tanking procedure Final go/no go round for launch Remote disconnection of the fluid umbilicals	Stay alert in case of an abort Possibility of manual umbilical disconnection and manual depressurization	

Mission/ Operational Phase		Appr. Time (Start)	Phase End	Payload	Aerostructure	Flightcomputer	Telemetry	Propulsion	Recovery	Recovery Team
Ignition		T-2s	The ignitor is burning			Transmits the signal through the electrical umbilical to the filling station	Receives the ignition signal and hands it to the flightcomputer	Ignitor is ignited		
Flight general	Lift-Off	T=0s	The rocket starts moving under its own thrust		Rail buttons provide stabilization on the launch rail	Open the main valve	Transmit rocket data and position	Booster fires after the main valve is opened		
	Power Ascent	T+0s	The rocket is no longer accelerating upwards	Start recording flight data		Measure flight parameters	Transmit rocket data and position			
	Supersonic Phase	T+7s	The rocket achieves supersonic velocity			Measure flight parameters	Transmit rocket data and position			
	Booster Burnout	T+8s	The rocket's oxidizer is fully consumed			Measure flight parameters	Transmit rocket data and position			
	Subsonic Phase	T+15s	The rocket flies ballistically at subsonic velocity		Air brake opens according to apogee estimation	Measure flight parameters and actuate airbrake	Transmit rocket data and position			
	Coast Phase	T+25	Apogee is detected by the flightcomputers		Air brake closes to ensure no further drag	Measure flight parameters and actuate airbrake	Transmit rocket data and position			
	Drogue Deploy-ment	T+45s	Drogue parachute is deployed	Film the drogue deployment for post launch analysis	Air brake opens to enhance drag	Trigger the drogue deployment	Confirm drogue deployment via data link		The gas capsules of the drogue deployment are punctured and separate the nosecone	
	Drogue Descent	T+47s	Reaching an altitude of 450 m	Measurement of cosmic radiation		Measure flight parameters	Transmit rocket data and position		The drogue parachute slows the rocket to 28 m/s	
	Main Deploy-ment	T+210s	Main parachute is deployed			Trigger the main deployment at 450 m	Transmit rocket data and position		The pyrotechnic charge opens the tender descenders, releasing the main parachute	
	Main Descent	T+242s	The rocket lands			Measure flight parameters	Transmit rocket data and position		The main parachute slows the rocket to 9 m/s	
	Landing	T+250s	The area is free for recovery operations				Transmit rocket data and position			

Mission/ Operational Phase		Appr. Time (Start)	Phase End	Assembly Tent Team	Mission Control Team	Launch Rail Team	Recovery Team
Post flight	Recovery	T+30 min	The rocket is brought into the assembly tent	Prepare to receive the rocket for final disassembly	Provide the recovery team with GNSS data Actuate the valves on the filling station to depressurize the system	Close the gas bottles Depressurize the filling station	Recover the rocket
	Disassembly	T+1h	The rocket, filling station, and all tools are stored	Disassembly of the rocket Storing of the rocket	Saving of all data First analysis of the data and final flight height Disassembly of the mission control	Disassembly of the launch rail Disassembly of the filling station	

4.1 Arming of the System

The procedure to arm the system on the launch pad consists of three individual phases. Firstly, the rocket is armed by tightening two arming screws in the upper part of the midsection and pulling out the arming pin. This marks the readiness of the REC system to be deployed. The next phase starts with opening the nitrogen and nitrous oxide bottles as well as the manual ox fill valves at the electrically controlled filling panel of the FS and closing the filling panel with the acrylic panel. In the final phase, the electrical connections between the FS, the Saftey Control Box, and the ignitor are established. Both the ignition key and the vent valve override key are inserted into the Saftey Control Box, but only the ignition key is turned, triggering both visual and auditory signals. This procedure enhances the safety of the operating crew at the launch rail by increasing the distance between them and the system during each phase of the process.

4.2 Abort Scenarios

For the launch sequence to be interrupted at any time before lift-off, the order of operations is flipped. First, the ignition is de-armed and with a possible data link obstruction, the vent valves located inside of the rocket can be manually overridden via the vent valve override key to manually depressurize the rocket. After successful depressurization of the rocket, the electrical connection to the ignitor is disconnected and the ignitor cables are shunted again. Next the gas bottles are closed and the filling panel is depressurized and purged via the manual vent valves. As the last step, the arming pin is reinserted, and the arming screws are loosened.

4.3 Thrust curves

Figure 4.1 shows an ensemble of measured thrust curves of all successful Hot-Fire tests. For the following flight simulations, the thrust curve of HF 6.1 was used, as it is the test closest to the needed total impulse and closely resembles the flight performance.

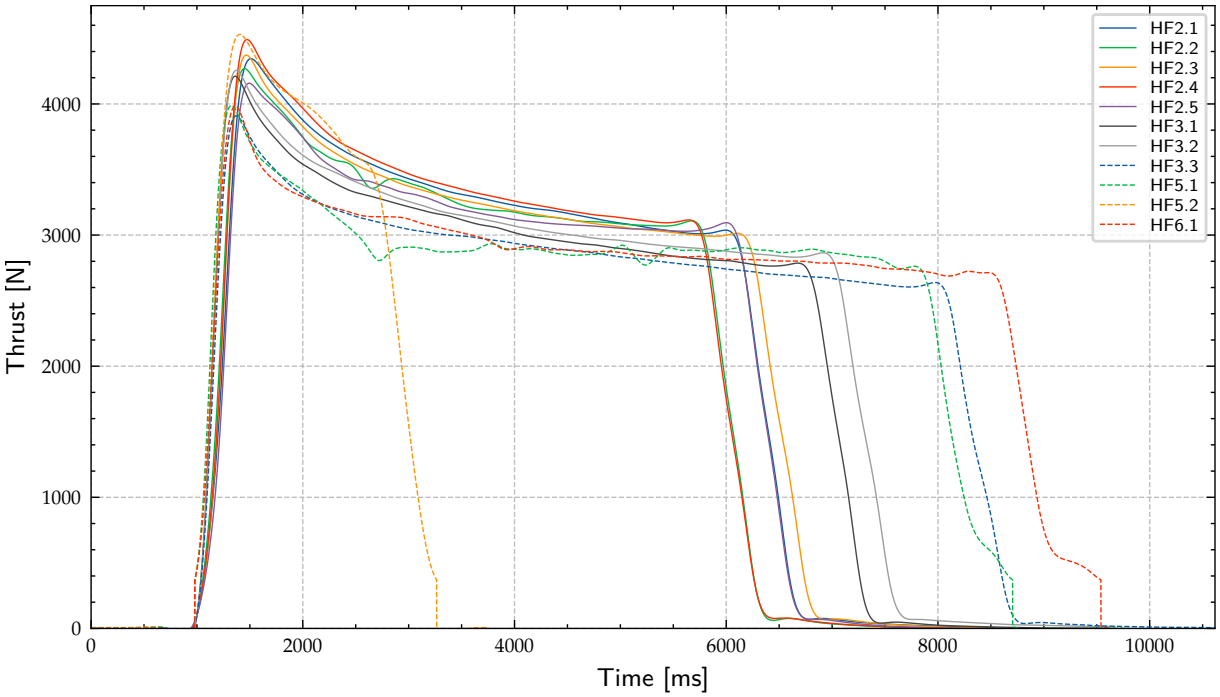

Figure 4.1: All thrust curves of the successful Hot-Fires. The thrust curves were filtered with butterworth filter (order=2, f_crit=20 MHz, python scipy, filtfilt function) for better visibility. The unfiltered thrust curves can be looked up in the corresponding test reports.

4.4 Tanking and Pressurizing

The tanking procedure involves the following steps:

- Pre-pressurizing to 18 bar
- Starting the fill hysteresis with a target pressure of 18 bar
- Opening the oxidizer fill valve, such that the pressure remains constant slightly above 18 bar
- As soon as liquid venting is visible at the lower vent valve, it is force-closed
- If liquid venting is visible at the upper vent valve, the oxidizer fill valve is closed
- The pressure settles at 18 bar
- In this state, the system is on standby until EuRoC gives the go for pressurization and launch
- A top-off is done: the oxidizer fill valve is opened until liquid venting, then closed again
- As soon as the pressure has leveled at 18 bar the fill hysteresis is stopped
- The oxidizer fill line is vented
- The oxidizer QD is disconnected
- By opening the first pressurizing fill valve, the pressurizing tank is pressurized to about 280 bar
- By opening the second fill valve, the pressurizing tank reaches close to 300 bar
- Both valves are closed and the N_2 fill line is vented
- The N_2 QD is disconnected

The tanking and pressurizing procedure is completed by disconnecting the N_2 QD and the rocket is ready for launch.

4.5 Flight Simulation

Figure 4.2 depicts the flight trajectory simulated with RocketPy for ALCEDO. As already seen in the Table 4.1 the whole flight cycle takes about 10 min. The required off-the-rail velocity by EuRoC can be achieved with the thrust curve given from Section 4.3.

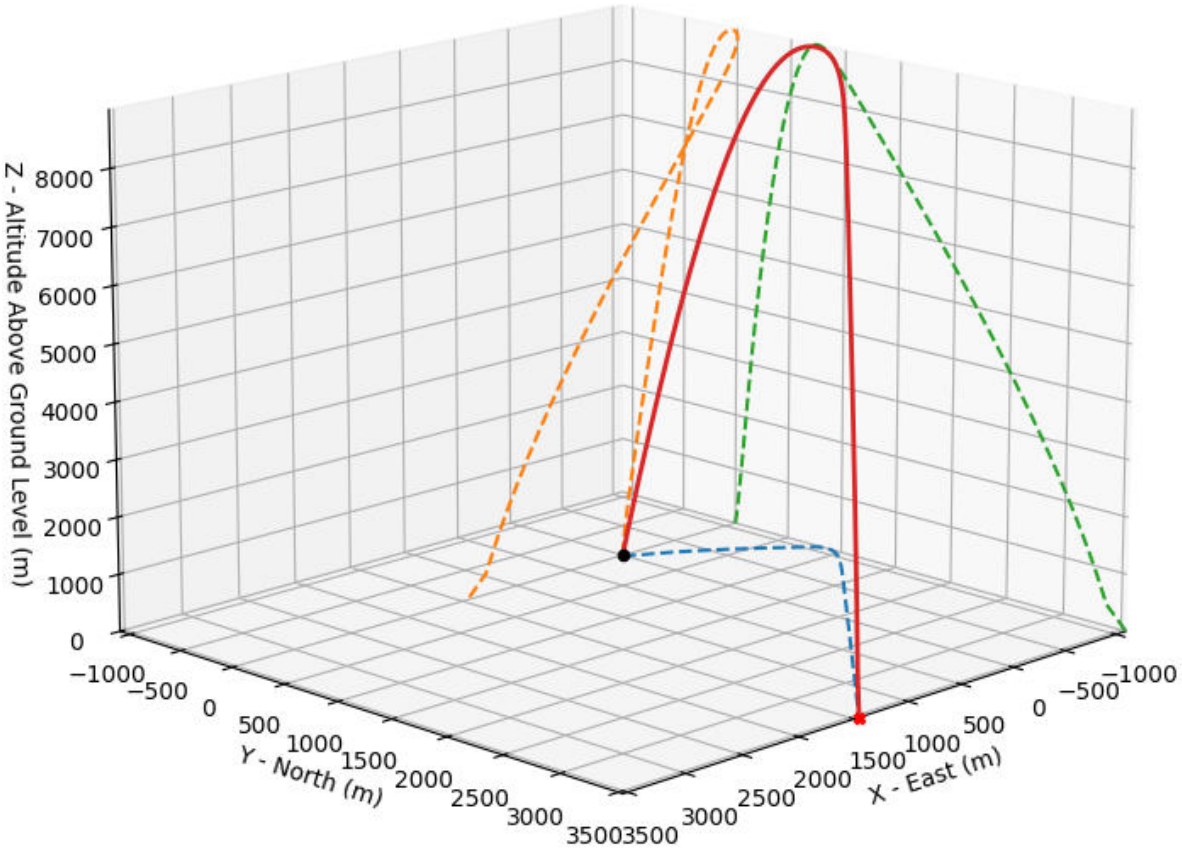

Figure 4.2: Flight trajectory of a ALCEDO flight with wind speed of 5.7 m/s at the surface scaling up linearly to 28.2 m/s

A few trajectories for different constant wind speeds were simulated. The key parameters are listed in Table 4.2

Table 4.2: Apogee, stabilities and drift distances at different surface speeds simulated with RocketPy, not including the air brake.

Side Wind [m/s]	Apogee [m]	Stability off Rail [calibers]	max. Stability [calibers]	Drift Distance [m]
0	9256	2.9	4.3	2152
2.5	9145	2.9	4.3	2167
5	9000	2.9	4.3	2160
7.5	8829	2.9	4.3	2107
10	8623	2.9	4.3	2037

5 Conclusions and Outlook

With the project ALCEDO, we were able to implement a lot of the experience gained from previous projects. Firstly the integration of all subsystems could be enhanced to a level where the space inside of the rocket and the weight of the subsystem were minimized. This starts from the REC subsystem, where both deployment mechanisms and also the mounting of the system were updated to be as lightweight as possible while still withstanding the expected loads. Next to the AVI section, with the compact FLI flight computer design, the ability to charge the custom-built battery pack already proved its use in the testing campaign. This feature ensures that the power inside of the rocket lasts for the flight as well as a period of time after landing. The TEL patch antenna rings, which were introduced last year, worked flawlessly and therefore were planned to be used for the whole telemetry and GNSS system of our SRAD and also the CATS Vega, in order to get rid of internal antennas as well as RF-transparent hull elements. Due to concerns from the officials, this additional antenna ring for the CATS Vega will not be implemented in the flight vehicle and a RF-transparent nose cone was implemented for the official tracking system. The PRO system takes about two thirds of the total length of the rocket and is more integrated, when compared to last year's rocket, HALCYON. The system has the capability to compete in the 9 km flight category as well as in the 3 km category, if the weather conditions may change on the launch pad. Also, adaptions regarding the longer burn time as well as the higher thrust, the combustion chamber as well as the used fuel grain were thoroughly tested.

Furthermore in this year's edition, ASTG will have the first air brake on a pressurized hybrid engine to fly up to 9 km. With the capability of ALCEDO to fly to either 3 km or 9 km, the control algorithm can be switched on the pad. The system is placed below the structural oxidizer tank and above the combustion chamber assembly. The feedpipe as well as the cables for the sensors and the tail cone camera fit tightly through the center.

For the launch support equipment, various updates were implemented. The mission control now features the capability for more users to simultaneously monitor the received data of the rocket as well as the FS. The FS, with updated electronics and a dual oxidizer line for faster tanking, allows for two nitrous oxide bottles as well as two nitrogen bottles. For the launch rail, our QD system for propellant loading was thoroughly tested and re-iterated for a reliable disconnect of both fluid lines.

One design challenge, that was encountered during testing was with the REC FD. The system failed to release the argon gas sufficiently fast enough to reliably eject the nosecone. The problem was found. The pin used to pierce the capsule, got stuck or got only partially retracted by the spring, so the gas flow was obstructed. By adapting the tip of the pin and developing a new 3D-printed Spacer Spring (TPU filament) this problem could be fixed and the ejection tests worked flawlessly. SD worked reliably and safely with the new ignitors after developing a stronger cover.

As in previous years mentioned, the desired test flight before the competition was planned to be done in late August, but due to difficulties regarding the bureaucracy and the final launch location, this attempt was scrubbed. It should be mentioned that the effort put into the planning of the test flight was high and seemed promising in the beginning, but in the final weeks beforehand, none of the organizations gave their final approval or did not even bother to answer our messages. So it is still a hurdle to find an adequate testing facility in Austria as well as in neighboring countries. With our SPATZ test rocket we tried to compensate for the scrubbed test flight of ALCEDO with two successful flights up to 130 m above ground level to estimate the terminal velocities of our parachutes.

List of Figures

List of Tables